Linear Parameter-Varying Controller Design for Four-Wheel Independently Actuated Electric Ground Vehicles With Active Steering Systems

Rongrong Wang, Hui Zhang, and Junmin Wang, *Member, IEEE*

***Abstract*— This paper presents a linear parameter-varying (LPV) control strategy to preserve stability and improve handling of a four-wheel independently actuated electric ground vehicle in spite of in-wheel motors and/or steering system faults. Different types of actuator faults including loss-of-effectiveness fault, additive fault, and the fault makes an actuator's control effect stuck-at-fixed-level, are considered simultaneously. To attenuate the effects of disturbance and address the challenging problem, a novel fault-tolerant (FT) robust linear quadratic regulator (LQR)-based H_∞ controller using the LPV method is proposed. With the LQR-based H_∞ control, the tradeoff between the tracking performance and the control input energy is achieved, and the effect from the external disturbance to the controlled outputs is minimized. The eigenvalue positions of the system matrix of the closed-loop system are also incorporated to tradeoff between the control inputs and the transient responses. The vehicle states, including vehicle yaw rate, lateral and longitudinal velocities, are simultaneously controlled to track their respective references. Simulations for different fault types and various driving scenarios are carried out with a high-fidelity, CarSim®, full-vehicle model. Simulation results show the effectiveness of the proposed FT control approach.**

***Index Terms*— Active steering system, electric ground vehicle, in-wheel/hub motor, linear parameter-varying (LPV) control.**

NOMENCLATURE

C_a	Aerodynamic drag coefficient.
C_f	Front cornering stiffness.
C_r	Rear cornering stiffness.
F_X	Longitudinal force acting on vehicle center of gravity.
F_{xi}	Longitudinal tire force of the ith wheel.
F_i	Lateral tire force of the ith wheel.
F_{yf}	Front lateral tire force.
F_{yr}	Rear lateral tire force.
M	Mass of the vehicle.
I	Wheel rotational inertia.
I_z	Yaw inertia of the vehicle.
R_{eff}	Tire effective rolling radius.
V_x	Vehicle longitudinal speed at center of gravity.
V_{rx}	Vehicle longitudinal speed reference.
V_y	Vehicle lateral speed at center of gravity.
Ω_z	Vehicle yaw rate.
Ω_{rz}	Vehicle yaw rate reference.
l_f	Distance from front axle to the center of gravity.
l_r	Distance from rear axle to the center of gravity.
l_s	Half of the track width.
ω_i	Wheel rotational speed of the ith wheel.
T_i	Motor torque of the ith in-wheel motor.
T_{di}	Desired motor torque of the ith in-wheel motor.
δ	Ground-wheel steering angle.
δ_h	Hand-wheel steering angle.
ΔM_z	Additional yaw moment generated with the longitudinal tire force difference.

Manuscript received January 11, 2013; revised May 12, 2013; accepted August 7, 2013. Manuscript received in final form August 9, 2013. Date of publication September 6, 2013; date of current version June 16, 2014. This work was supported in part by the Office of Naval Research Young Investigator Program ONR-YIP Award under Grant N00014-09-1-1018, in part by Honda-OSU Partnership Program, and in part by OSU Transportation Research Endowment Program. Recommended by Associate Editor K. Butts.

R. Wang is with the School of Mechanical Engineering, Southeast University, Nanjing 211189, China (e-mail: wrr06fy@gmail.com).

H. Zhang and J. Wang are with the Department of Mechanical and Aerospace Engineering, The Ohio State University, Columbus, OH 43210 USA (e-mail: huizhang285@gmail.com; wang.1381@osu.edu).

Color versions of one or more of the figures in this paper are available online at http://ieeexplore.ieee.org.

Digital Object Identifier 10.1109/TCST.2013.2278237

I. INTRODUCTION

FOUR-WHEEL independently actuated (FWIA) electric ground vehicle is a promising vehicle architecture due to its actuation flexibility [1], [2]. Each of the wheels in an FWIA electric ground vehicle is independently driven by an in-wheel (or hub) motor. Thus, the additional yaw moment can be easily generated with torque differences between the left and right wheels because of the fast response of the in-wheel motor torque. Such an actuation flexibility facilitates the vehicle lateral motion control and helps the driver in avoiding some unintended lane departures [1]–[3]. Active steering has been considered to be another effective way of enhancing vehicle driving safety, improving driver's comfort and handling, because of the fast and precise steering intervention compared with the limited reaction time of the driver [4], [5]. A typical active steering system is a steering-by-wire system in which the mechanical link between the driver's action and the steering wheels has been removed and replaced with an electronically controlled actuator [5], [6]. The induced external yaw moment generated with torque differences between the left and right wheels, together with the automatic steering from a steer-by-wire system, make it possible to simultaneously regulate the vehicle lateral velocity and track the desired yaw rate.

Numerous research papers have been devoted to either the FWIA electric ground vehicle control or active steering

control designs [3]–[5], [7]–[10]. However, the study on the control of vehicle motions in the presence of both means of actuation is limited. The performance and stability of an FWIA vehicle heavily depend on the proper operations of the in-wheel motors. When an in-wheel motor fault occurs, the faulty wheel may fail to provide the expected torque and jeopardize the vehicle motion control [7], [8]. Thus, a fault-tolerant (FT) control system is safety-critical in FWIA electric ground vehicles. A few FT control methods for electric ground vehicles have been previously proposed in the literature, but a few of them are specifically designed for FWIA vehicles or some limited types of actuator faults are considered [11]–[13]. Adaptive control and sliding mode control-based FT controllers for an FWIA electric ground vehicle were proposed in [7] and [8], but only one type of in-wheel motor fault, i.e., loss-of-effectiveness fault was investigated. An optimal controller considering the loss-of-effective fault and actuator failure for FT path-tracking control of a four-wheel-steering-driving electric vehicle is reported in [14]. As the faulty actuator control effectiveness will become zero if the corresponding actuator is in failure, actuator failure may be treated as a special case of loss-of-effective fault. The fault considered in [14] is thus also a loss-of-effective fault As the fault information, such as the fault type, is usually unknown, it may be limited to design a FT controller for a specified fault. For this reason, it is more desirable to develop a FT controller, which can deal with different kinds of actuator faults [15]. A problem associated with the steer-by-wire system is that if the mechanical connection between steering wheel and road wheel is removed, a fault from a sensor or actuator may result in unwanted steering effects and jeopardize the vehicle motion [16], [17]. To overcome the abovementioned potential issue, FT controllers are employed in steer-by-wire systems to tolerate faults and maintain the desired vehicle stability and performance. For example, hardware or analytical redundancy-based methods are proposed in [6] and [16]–[18]. Dual-motor, dual-microcontroller control system architectures for steering-by-wire system have been adopted in [6] and [16]. Aiming to reduce the total number of redundant sensors, analytical redundancy-based methods for fault tolerance of steering-by-wire systems are proposed in [17] and [18]. Although the abovementioned research efforts were successful, the FT control of an FWIA electric ground vehicle equipped with an active steering system has seldom been studied.

The fault diagnosis mechanism is difficult to design for multiactuator systems and overactuated systems [19]. Nevertheless, the passive FT controller does not require exact actuator fault information, and thus is suitable to implement on an FWIA electric ground vehicle. In this paper, a passive FT control for an FWIA electric ground vehicle equipped with an active steering system to preserve the closed-loop stability in spite of in-wheel motor or steering system faults is proposed. It is well known that some nonlinear systems can be approximated by linear parameter-varying (LPV) systems, and then the well-developed techniques designed for linear systems can be applied to the approximated models. The main contributions of this paper lie in the following aspects.

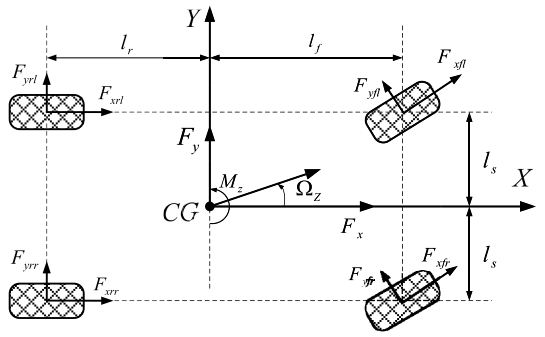

Fig. 1. Schematic diagram of a vehicle planar motion model.

1) Three most common types of actuator faults, i.e., loss-of-effectiveness fault, additive fault, and the fault makes an actuator's control effect stuck-at-fixed-level [15], for both of the in-wheel motors and steering system are investigated.
2) A robust linear quadratic regulator (LQR)-based H_∞ control is proposed to deal with the actuator faults, which are described via the norm-bounded uncertainties. With the LQR-based H_∞ control, the tradeoff between the tracking performance and the control inputs can be achieved, and the effect from the external input to the controlled output is minimized. Furthermore, because of the physical limitations on the actuators, to have better transient responses, the control inputs are also restricted by constraining all the eigenvalues of the closed-loop system into a disk.
3) External yaw moment, ground-wheel steering angle, and total motor torque are designed to simultaneously regulate the desired yaw rate and track the vehicle lateral and longitudinal velocity references in spite of in-wheel motor or/and steering system faults.
4) As the tire cornering stiffness can be affected by several factors such as tire-road friction coefficient (TRFC), tire normal force, and so on [20], the uncertainties in the tire cornering stiffness are also considered in the controller design, making the proposed FT controller robust to the tire force modeling error.

The rest of this paper is organized as follows. The system model and problem formulation are presented in Section II. The passive FT controller is designed and analyzed in Section III. Simulation results for different fault types and various driving scenarios based on a high-fidelity, CarSim®, full-vehicle model are presented in Section IV followed by conclusive remarks.

II. System Modeling and Problem Formulation

A. Vehicle Model

Different from the conventional vehicle architectures, an external vehicle yaw moment can be easily generated in an FWIA vehicle to control the vehicle yaw and lateral motions. Ignoring the pitch and roll motions, the vehicle has three planar degrees of freedom for longitudinal motion, lateral motion, and yaw motion. A schematic diagram of the vehicle model is

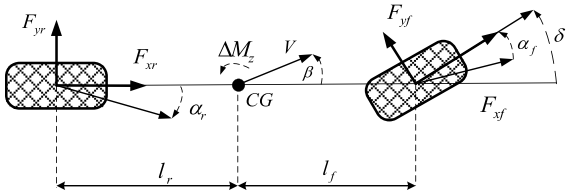

Fig. 2. Schematic diagram of the bicycle model with external yaw moment.

shown in Fig. 1. We can see from this figure that the external yaw moment ΔM_z can be generated with the longitudinal tire force difference between the left and right wheels. The external yaw moment can be calculated as [21]

$$\Delta M_Z = (F_{\mathrm{xfl}}\cos\delta + F_{\mathrm{xrl}})\, l_s - (F_{\mathrm{xfr}}\cos\delta + F_{\mathrm{xrr}})\, l_s \quad (1)$$

where δ is the steering angle of the front wheels and F_{xi} is the longitudinal tire force of the ith wheel.

To simplify the controller design, a bicycle model [23] shown in Fig. 2 is adopted to model the vehicle lateral and yaw motions. Considering the external yaw moment ΔM_z generated with the longitudinal tire force differences between the left and right wheels, the vehicle can be modeled as [1], [20]

$$\begin{cases} \dot{V}_x = V_y\Omega_z - \frac{C_a}{M}V_x^2 + \frac{1}{M}F_X \\ \dot{V}_y = -V_x\Omega_z + \frac{1}{M}\left(F_{\mathrm{yf}}\cos\delta + F_{\mathrm{yr}}\right) \\ \dot{\Omega}_z = \frac{1}{I_z}\left(l_f F_{\mathrm{yf}}\cos\delta - l_r F_{\mathrm{yr}}\right) + \frac{1}{I_z}\Delta M_z \end{cases} \quad (2)$$

where V_x and V_y are the longitudinal speed and lateral speed, respectively, Ω_z is the yaw rate, M is the mass of the vehicle, I_z is the vehicle yaw inertia, and C_a is the aerodynamic drag term.

The front and rear lateral forces can be written as

$$F_{\mathrm{yf}} = F_{\mathrm{yfl}} + F_{\mathrm{yrl}},\ F_{\mathrm{yr}} = F_{\mathrm{yrr}} + F_{\mathrm{yrl}} \quad (3)$$

with F_{yi} being the lateral tire force of the ith wheel, F_X is the total longitudinal force generated by all the four tires, and can be calculated by

$$F_X = (F_{\mathrm{xfl}} + F_{\mathrm{xfr}})\cos\delta + F_{\mathrm{xrl}} + F_{\mathrm{xrr}} - \left(F_{\mathrm{yfl}} + F_{\mathrm{yfr}}\right)\sin\delta. \quad (4)$$

Note that the vehicle model (2) can be further written as

$$\begin{cases} \dot{V}_x = V_y\Omega_z - \frac{C_a}{M}V_x^2 + \frac{1}{M}F_X \\ \dot{V}_y = -V_x\Omega_z + \frac{1}{M}\left(F_{\mathrm{yf}} + F_{\mathrm{yr}}\right) + \frac{1}{M}F_{\mathrm{yf}}\,(\cos\delta - 1) \\ \dot{\Omega}_z = \frac{1}{I_z}\left(l_f F_{\mathrm{yf}} - l_r F_{\mathrm{yr}}\right) + \frac{l_f}{I_z}F_{\mathrm{yf}}\,(\cos\delta - 1) + \frac{1}{I_z}\Delta M_z. \end{cases} \quad (5)$$

The front and rear lateral forces can be modeled as [23]

$$F_{\mathrm{yf}} = C_f\alpha_f, \quad F_{\mathrm{yr}} = C_r\alpha_r \quad (6)$$

where $C_{\mathrm{f,r}}$ are the tire cornering stiffness values and $\alpha_{\mathrm{f,r}}$ are the tire slip angles that can be expressed as [21]

$$\alpha_f = \delta - \frac{V_y + \Omega_z l_f}{V_x}, \quad \alpha_r = \frac{\Omega_z l_r - V_y}{V_x}. \quad (7)$$

The rotational dynamics of each wheel can be represented by

$$I\dot{\omega}_i = -R_{\mathrm{eff}}F_{\mathrm{xi}} + T_i \quad (8)$$

where I is the wheel moment of inertia, R_{eff} is the tire rolling radius, and T_i is the torque of the ith in-wheel motor. In general, if a fault occurs to a certain motor and/or the motor driver, the corresponding motor torque will be different from the desired value, T_{di}, or stay at a fixed value. With the rotational dynamics in (8), the longitudinal tire force at each tire can be written as

$$F_{\mathrm{xi}} = \frac{T_i - I\dot{\omega}_i}{R_{\mathrm{eff}}}. \quad (9)$$

Denoting three virtual control inputs as

$$\begin{cases} u_1 = T_{\mathrm{fl}}\cos\delta + T_{\mathrm{rl}} \\ u_2 = T_{\mathrm{fr}}\cos\delta + T_{\mathrm{rr}} \\ u_3 = \delta \end{cases} \quad (10)$$

the overall vehicle model (5) can be written as

$$\begin{cases} \dot{V}_x = V_y\Omega_z - \frac{C_a}{M}V_x^2 + \frac{1}{MR_{\mathrm{eff}}}(u_1 + u_2) + d_1 \\ \dot{V}_y = -\frac{(C_f + C_r)V_y}{MV_x} + \left(\frac{C_r l_r - C_f l_f}{MV_x} - V_x\right)\Omega_z + \frac{C_f}{M}u_3 + d_2 \\ \dot{\Omega}_z = \frac{(C_r l_r - C_f l_f)V_y - \left(C_f l_f^2 + C_r l_r^2\right)\Omega_z}{I_z V_x} + \frac{C_f l_f}{I_z}u_3 \\ \qquad + \frac{l_s}{I_z R_{\mathrm{eff}}}(u_1 - u_2) + d_3 \end{cases} \quad (11)$$

where d_* is the unmodeled terms and can be written as

$$\begin{cases} d_1 = \frac{1}{M}F_{\mathrm{yf}}\sin\delta + \frac{I}{MR_{\mathrm{eff}}}\left[\cos\delta\ \ \cos\delta\ 1\ 1\right]\dot{\omega} \\ d_2 = \frac{1}{M}F_{\mathrm{yf}}\,(\cos\delta - 1) \\ d_3 = \frac{l_f}{I_z}F_{\mathrm{yf}}\,(\cos\delta - 1) + \frac{l_s I}{I_z R_{\mathrm{eff}}}\left[\cos\delta - \cos\delta\ 1 - 1\right]\dot{\omega} \end{cases} \quad (12)$$

with $\omega = [\omega_{\mathrm{fl}}\ \omega_{\mathrm{fr}}\ \omega_{\mathrm{rl}}\ \omega_{\mathrm{rr}}]^T$. Note that in (10), u_1 and u_2 are the total motor torque values in the vehicle longitudinal direction on the left and right sides of the vehicle, respectively. u_3 is the front wheel steering angle.

Remark 1: At high vehicle speeds, where the active vehicle motion control is more necessary, the ground-wheel steering angle δ is usually small and thus are the values of $F_{\mathrm{yf}}\sin\delta$ and $F_{\mathrm{yf}}(\cos\delta - 1)$. So these two terms are not considered in the vehicle model (11). Omitting these two terms in the modeling can facilitate the controller design and thus is beneficial for the real-time implementation purpose. Because of the measurement noise, directly using the time derivative of a wheel angular speed signal may be challenging. As the value of $\dot{\omega}$ is usually small in normal driving, it is not considered in the modeling but placed into the disturbance terms. A robust LQR-based H_∞ controller will be designed to attenuate the effects of disturbance and unmodeled dynamics.

B. Fault Model

If an actuator fault occurs, the actual control effort v_i from an actuator will be different to its desired one. In this paper, the three most common types of actuator faults, i.e., loss-of-effectiveness fault, additive fault, and the fault makes an actuator's control effect stuck-at-fixed-level are studied. To model all of these fault types in a generalized way, we introduce the following actuator fault model:

$$v_i = \eta_i v_{\mathrm{di}} + \Delta v_i \quad (13)$$

where v_{di} is the desired control effort of an actual actuator, $0 < \eta_i \leq 1$ are time-varying parameters, Δv_i are unknown disturbances caused by the faults.

With the actuator fault model (13), faults of the virtual control inputs described by (10) can be modeled as

$$\begin{cases} u_1 = \lambda_1 u_{d1} + \Delta u_1 \\ u_2 = \lambda_2 u_{d2} + \Delta u_2 \\ u_3 = \lambda_3 u_{d3} + \Delta u_3 \end{cases} \tag{14}$$

where λ_i $(i = 1, 2, 3)$ are time-varying parameters and satisfy $0 < \lambda_i \leq 1$. The desired virtual control efforts can be written as

$$\begin{cases} u_{d1} = T_{dfl} \cos\delta_d + T_{drl} \\ u_{d2} = T_{dfr} \cos\delta_d + T_{drr} \\ u_{d3} = \delta_d \end{cases}$$

with T_{dj} $(j = fr, fl, rl, rr)$ being the desired motor torques and δ_d being the desired front wheel steering angle.

Remark 2: Note that different types of actuator faults can be all described by (13). For example, if an additive fault occurs to an in-wheel motor, the torque of the faulty in-wheel motor can be written as $T_f = T_{\mathrm{df}} + \Delta T_f$ with T_{df} being the desired motor torque of the faulty motor and ΔT_f being the added torque. So for the virtual control effort u_i which includes the faulty motor torque T_f, we have $\lambda_i = 1$ and $\Delta u_i \neq 0$. If a loss-of-effectiveness fault occurs to an in-wheel motor, we have $T_f = \eta_f T_{\mathrm{df}}$ with $0 < \eta_f < 1$. With the definition of u_1 and u_2 in (10), we can reach $\Delta u_i = 0$ and the parameter λ_i satisfies $0 < \lambda_i < 1$ in this case. If one of the in-wheel motor torque values stuck at a fixed level, we have $T_f = c$ with c being a constant, and thus $0 < \lambda_i < 1$ and $\Delta u_i \neq 0$.

Remark 3: For the steering system with hardware redundancy such as the dual-motor-and-dual-microcontroller steering architecture [17], the faulty steering system control effort can still be modeled by the third equation in (14). Specifically, if an additive torque applies to one of the steering motor torques, we have $\lambda_3 = 1$ and $\Delta u_3 \neq 0$. If a loss-of-effectiveness fault occurs to a steering motor, we have $0 < \lambda_3 < 1$ and $\Delta u_3 = 0$. If one of the steering motor torque values is stuck at a fixed level, then $0 < \lambda_3 < 1$ and $\Delta u_3 \neq 0$.

Remark 4: For the steering system without actuation redundancy, i.e., the steering system has only one steering motor, if the steering motor is in a failure, we have $\lambda_3 = 0$ and $\Delta u_3 = 0$. If a fault which makes the steering motor torque shuck at a fixed level occurs, we have $\lambda_3 = 0$ and $\Delta u_3 = c_3$ with c_3 being a constant. In these two cases, the front wheel steering angle will not contribute to the control authority, which means that the vehicle yaw rate cannot be controlled if there is no intervention from the external yaw moment. The yaw rate of an FWIA vehicle, however, may still be regulated with the external yaw moment generated by the torque differences between the left and right side in-wheel motors. Simulation results will show that acceptable control performance may still be achieved even if the front wheel steering angle cannot be adjusted. Note that if the loss-of-effectiveness fault occurs to the steering-by-wire system without hardware redundancy, we still have $0 < \lambda_3 < 1$ and $\Delta u_3 = 0$.

C. Vehicle Model Considering Actuator Faults

Denote $\boldsymbol{x} = [V_x \;\; V_y \;\; \Omega_z]^T$, $\boldsymbol{u} = [u_{d1} \;\; u_{d2} \;\; u_{d3}]^T$, $\boldsymbol{\Lambda} = \mathrm{diag}[\lambda_1 \; \lambda_2 \; \lambda_3]$, and $\boldsymbol{d} = [d_1 \; d_2 \; d_3]^T$. With (11) and (14), the vehicle model can be written as

$$\dot{\boldsymbol{x}} = \boldsymbol{A}\boldsymbol{x} + \boldsymbol{B}\boldsymbol{\Lambda}\boldsymbol{u} + \boldsymbol{B}\boldsymbol{w} + \boldsymbol{d} \tag{15}$$

where $\boldsymbol{w} = [\Delta u_1 \;\; \Delta u_2 \;\; \Delta u_3]^T$

$$\boldsymbol{A} = \begin{bmatrix} \frac{-V_x C_a}{M} & \Omega_z & 0 \\ 0 & -\frac{C_f + C_r}{M V_x} & \frac{C_r l_r - C_f l_f}{M V_x} - V_x \\ 0 & \frac{C_r l_r - C_f l_f}{V_x I_z} & \frac{-C_r l_r^2 - C_f l_f^2}{V_x I_z} \end{bmatrix}$$

$$\boldsymbol{B} = \begin{bmatrix} \frac{1}{M R_{\mathrm{eff}}} & \frac{1}{M R_{\mathrm{eff}}} & 0 \\ 0 & 0 & \frac{C_f}{M} \\ \frac{l_s}{I_z R_{\mathrm{eff}}} & -\frac{l_s}{I_z R_{\mathrm{eff}}} & \frac{C_f l_f}{I_z} \end{bmatrix}.$$

It is necessary to mention that the system in (15) is nonlinear. To facilitate the controller design, we convert the nonlinear system into an LPV system. As V_x and Ω_z are time-varying but measurable, we choose the three auxiliary time-varying parameters vector as $\rho_1(t) = V_x$, $\rho_2(t) = \Omega_z$, and $\rho_3(t) = 1/V_x$. Denoting $\boldsymbol{\rho} = [\rho_1 \;\; \rho_2 \;\; \rho_3]^T$, the vehicle model (15) can be rewritten as

$$\dot{\boldsymbol{x}} = \boldsymbol{A}(\boldsymbol{\rho})\boldsymbol{x} + \boldsymbol{B}\boldsymbol{\Lambda}\boldsymbol{u} + \boldsymbol{B}\boldsymbol{w} + \boldsymbol{d} \tag{16}$$

where

$$\boldsymbol{A}(\boldsymbol{\rho}) = \begin{bmatrix} -\frac{\rho_1 C_a}{M} & \rho_2 & 0 \\ 0 & -\rho_3 \frac{C_f + C_r}{M} & \rho_3 \frac{C_r l_r - C_f l_f}{M} - \rho_1 \\ 0 & \rho_3 \frac{C_r l_r - C_f l_f}{I_z} & -\rho_3 \frac{C_r l_r^2 + C_f l_f^2}{I_z} \end{bmatrix}.$$

Normally, the tire cornering stiffness is treated as a constant parameter to facilitate the controller design [13], [14]. It is important to note here that the tire cornering stiffness can be affected by many factors such as the TRFC, tire normal force, wear of the tires, and so on [20]. The tire lateral forces calculated with a preselected cornering stiffness may not be accurate, so the uncertainties in the tire cornering stiffness are considered in this paper. Denoting

$$C_{\mathrm{m}f} = \frac{C_{\max f} + C_{\min f}}{2}, \quad C_{\mathrm{m}r} = \frac{C_{\max r} + C_{\min r}}{2} \tag{17}$$

with $C_{\max k}$ and $C_{\min k}$ being the maximal and minimal values of C_k $(k = f, r)$, respectively. The tire cornering stiffness can be written as

$$C_f = C_{\mathrm{m}f} + N_f \tilde{C}_f, \quad C_r = C_{\mathrm{m}r} + N_r \tilde{C}_r \tag{18}$$

where $\tilde{C}_f = C_{\max f} - C_{\mathrm{m}f}$, $\tilde{C}_r = C_{\max r} - C_{\mathrm{m}r}$ and N_f and N_r are time-varying parameters and satisfy $|N_k(t)| < 1$. Similarly, the aerodynamic drag term C_a can be written as

$$C_a = C_{\mathrm{m}a} + N_a \tilde{C}_a \tag{19}$$

where N_a is a time-varying parameter and satisfy $|N_a(t)| < 1$, $C_{\mathrm{m}a} = (C_{\max a} + C_{\min a})/2$ with $C_{\max a}$ and $C_{\min a}$ being the maximal and minimal values of C_a, respectively. With these new notations, $\boldsymbol{A}(\boldsymbol{\rho})$ and $\boldsymbol{B}$ in (16) can be rewritten as

$$\boldsymbol{A}(\boldsymbol{\rho}) = \boldsymbol{A_0}(\boldsymbol{\rho}) + \boldsymbol{\Delta A}(\boldsymbol{\rho}), \quad \boldsymbol{B} = \boldsymbol{B_0} + \boldsymbol{\Delta B} \tag{20}$$

with

$$\boldsymbol{A_0} = \begin{bmatrix} -\frac{\rho_1 C_{\mathrm{m}a}}{M} & \rho_2 & 0 \\ 0 & -\rho_3 \frac{C_{\mathrm{m}f}+C_{\mathrm{m}r}}{M} & \rho_3 \frac{C_{\mathrm{m}r}l_r - C_{\mathrm{m}f}l_f}{M} - \rho_1 \\ 0 & \rho_3 \frac{C_{\mathrm{m}r}l_r - C_{\mathrm{m}f}l_f}{I_z} & -\rho_3 \frac{C_{\mathrm{m}r}l_r^2 + C_{\mathrm{m}f}l_f^2}{I_z} \end{bmatrix}$$

$$\boldsymbol{\Delta} A(\boldsymbol{\rho}) = \begin{bmatrix} -\frac{\rho_1 N_a \tilde{C}_a}{M} & 0 & 0 \\ 0 & -\rho_3 \frac{N_f \tilde{C}_f + N_r \tilde{C}_r}{M} & \rho_3 \frac{N_r \tilde{C}_r l_r - N_f \tilde{C}_f l_f}{M} \\ 0 & \rho_3 \frac{N_r \tilde{C}_r l_r - N_f \tilde{C}_f l_f}{I_z} & -\rho_3 \frac{N_r \tilde{C}_r l_r^2 + N_f \tilde{C}_f l_f^2}{I_z} \end{bmatrix}$$

$$\boldsymbol{B_0} = \begin{bmatrix} \frac{1}{M R_{\mathrm{eff}}} & \frac{1}{M R_{\mathrm{eff}}} & 0 \\ 0 & 0 & \frac{C_{\mathrm{m}f}}{M} \\ \frac{l_s}{I_z R_{\mathrm{eff}}} & -\frac{l_s}{I_z R_{\mathrm{eff}}} & \frac{C_{\mathrm{m}f} l_f}{I_z} \end{bmatrix}$$

$$\boldsymbol{\Delta B} = \begin{bmatrix} 0 & 0 & 0 \\ 0 & 0 & \frac{N_f \tilde{C}_f}{M} \\ 0 & 0 & \frac{N_f \tilde{C}_f l_f}{I_z} \end{bmatrix}.$$

If we take $N_f = N_r$, then the vehicle model can be further written as

$$\begin{aligned} \dot{\boldsymbol{x}} &= (\boldsymbol{A_0}(\boldsymbol{\rho}) + \boldsymbol{\Delta A}(\boldsymbol{\rho}))\boldsymbol{x} + (\boldsymbol{B_0} + \boldsymbol{\Delta B})\boldsymbol{\Lambda u} + (\boldsymbol{B_0} + \boldsymbol{\Delta B})\boldsymbol{w} + \boldsymbol{d} \\ &= \left(\boldsymbol{A_0}(\boldsymbol{\rho}) + \tilde{\boldsymbol{A}}(\boldsymbol{\rho})\boldsymbol{N_1}\right)\boldsymbol{x} + \left(\boldsymbol{B_0} + \tilde{\boldsymbol{B}}\boldsymbol{N_1}\right)\boldsymbol{\Lambda u} + \left(\boldsymbol{B_0} + \tilde{\boldsymbol{B}}\boldsymbol{N_1}\right)\boldsymbol{w} + \boldsymbol{d} \end{aligned} \tag{21}$$

where

$$\tilde{\boldsymbol{A}}(\boldsymbol{\rho}) = \begin{bmatrix} -\rho_1 \frac{N_a \tilde{C}_a}{M} & 0 & 0 \\ 0 & -\rho_3 \frac{\tilde{C}_f + \tilde{C}_r}{M} & \rho_3 \frac{\tilde{C}_r l_r - \tilde{C}_f l_f}{M} \\ 0 & \rho_3 \frac{\tilde{C}_r l_r - \tilde{C}_f l_f}{I_z} & -\rho_3 \frac{\tilde{C}_r l_r^2 + \tilde{C}_f l_f^2}{I_z} \end{bmatrix}$$

$$\tilde{\boldsymbol{B}} = \begin{bmatrix} 0 & 0 & 0 \\ 0 & 0 & \frac{\tilde{C}_f}{M} \\ 0 & 0 & \frac{\tilde{C}_r l_f}{I_z} \end{bmatrix}$$

$$\boldsymbol{N_1} = \begin{bmatrix} N_a & 0 & 0 \\ 0 & N_r & 0 \\ 0 & 0 & N_r \end{bmatrix}.$$

By considering the uncertainties in the tire cornering stiffness and the aerodynamic drag term, we have obtained the LPV system with uncertainties in (21).

Remark 5: Note that the assumption $\boldsymbol{N}_f = \boldsymbol{N}_r$ is used. As the road conditions are usually uniform to the front and rear wheels, it is reasonable to assume that the road coherent coefficients for both tires are identical. If the assumption is not used, $\boldsymbol{\Delta A}(\boldsymbol{\rho})$ can be written as

$$\boldsymbol{\Delta A}(\boldsymbol{\rho}) = \tilde{\boldsymbol{A}}'(\boldsymbol{\rho})\boldsymbol{N}' + \tilde{\boldsymbol{A}}''(\boldsymbol{\rho})\boldsymbol{N}''$$

with

$$\tilde{\boldsymbol{A}}(\boldsymbol{\rho}) = \begin{bmatrix} 0 & 0 & 0 \\ 0 & -\rho_3 \frac{\tilde{C}_f}{M} & \rho_3 \frac{\tilde{C}_r l_r}{M} \\ 0 & \rho_3 \frac{-\tilde{C}_f l_f}{I_z} & -\rho_3 \frac{\tilde{C}_r l_r^2}{I_z} \end{bmatrix}$$

$$\boldsymbol{N}' = \begin{bmatrix} N_a & 0 & 0 \\ 0 & N_f & 0 \\ 0 & 0 & N_r \end{bmatrix}$$

$$\tilde{\boldsymbol{A}}''(\boldsymbol{\rho}) = \begin{bmatrix} 0 & 0 & 0 \\ 0 & -\rho_3 \frac{\tilde{C}_r}{M} & \rho_3 \frac{-\tilde{C}_f l_f}{M} \\ 0 & \rho_3 \frac{\tilde{C}_r l_r}{I_z} & -\rho_3 \frac{\tilde{C}_f l_f^2}{I_z} \end{bmatrix}$$

$$\boldsymbol{N}'' = \begin{bmatrix} N_a & 0 & 0 \\ 0 & N_r & 0 \\ 0 & 0 & N_f \end{bmatrix}.$$

The controller can also be designed in a similar fashion. However, the assumption $\boldsymbol{N}_f = \boldsymbol{N}_r$ can greatly simplify the controller design process.

III. Fault-Tolerant Tracking Controller Design

In the previous section, we have formulated the vehicle model with a generalized actuator fault description. From the application perspective, it is always desired that the system states in (21) can track the prescribed references. In this section, we propose the tracking controller design method.

Denoting the reference as $\boldsymbol{r}$, also defining $\boldsymbol{\xi} = \left[\boldsymbol{\xi}_1\ \boldsymbol{\xi}_2\right]^T$ with $\boldsymbol{\xi}_1 = \boldsymbol{x} - \boldsymbol{r}$ and $\boldsymbol{\xi}_2 = \int_0^t (\boldsymbol{x} - \boldsymbol{r})dt$, the original system (21) can be rewritten as

$$\begin{aligned} \dot{\boldsymbol{\xi}} &= \begin{bmatrix} \boldsymbol{A_0}(\boldsymbol{\rho}) + \tilde{\boldsymbol{A}}(\boldsymbol{\rho})\boldsymbol{N_1} & \boldsymbol{0} \\ \boldsymbol{I} & \boldsymbol{0} \end{bmatrix}\boldsymbol{\xi} + \begin{bmatrix} \boldsymbol{B_0} + \tilde{\boldsymbol{B}}\boldsymbol{N_1} \\ \boldsymbol{0} \end{bmatrix}\boldsymbol{\Lambda u} \\ &\quad + \begin{bmatrix} \boldsymbol{B_0} + \tilde{\boldsymbol{B}}\boldsymbol{N_1} \\ \boldsymbol{0} \end{bmatrix}\boldsymbol{w} + \boldsymbol{d}_{\boldsymbol{\xi}} \end{aligned} \tag{22}$$

with $\boldsymbol{d}_{\boldsymbol{\xi}} = [\,\boldsymbol{d}^T\ -\dot{\boldsymbol{r}}^T\ -\boldsymbol{r}^T\,]^T$.

In this paper, to achieve a better control performance, we propose the designing of a gain-scheduling state-feedback controller for the system in (22) as

$$\boldsymbol{u} = \boldsymbol{K}(\boldsymbol{\rho})\boldsymbol{\xi} \tag{23}$$

where $\boldsymbol{K}(\boldsymbol{\rho})$ is the gain to be designed. With the advanced sensing technologies, such as global positioning system (GPS) and inertia measurement unit, the vehicle states V_x, V_y, and Ω_z can be accurately measured [21], [22]. With (23), the system model (22) can be rewritten as

$$\begin{aligned} \dot{\boldsymbol{\xi}} &= \begin{bmatrix} \boldsymbol{A_0}(\boldsymbol{\rho}) + \tilde{\boldsymbol{A}}(\boldsymbol{\rho})\boldsymbol{N_1} & \boldsymbol{0} \\ \boldsymbol{I} & \boldsymbol{0} \end{bmatrix}\boldsymbol{\xi} + \begin{bmatrix} \boldsymbol{B_0} + \tilde{\boldsymbol{B}}\boldsymbol{N_1} \\ \boldsymbol{0} \end{bmatrix}\boldsymbol{\Lambda K}(\boldsymbol{\rho})\boldsymbol{\xi} \\ &\quad + \begin{bmatrix} \boldsymbol{B_0} + \tilde{\boldsymbol{B}}\boldsymbol{N_1} \\ \boldsymbol{0} \end{bmatrix}\boldsymbol{w} + \boldsymbol{d}_{\boldsymbol{\xi}} \\ &= \left(\begin{bmatrix} \boldsymbol{A_0}(\boldsymbol{\rho}) & \boldsymbol{0} \\ \boldsymbol{I} & \boldsymbol{0} \end{bmatrix} + \begin{bmatrix} \tilde{\boldsymbol{A}}(\boldsymbol{\rho}) \\ \boldsymbol{0} \end{bmatrix}\boldsymbol{N_1}\,[\boldsymbol{I}\ \ \boldsymbol{0}] + \begin{bmatrix} \boldsymbol{B_0} \\ \boldsymbol{0} \end{bmatrix}\boldsymbol{\Lambda K}(\boldsymbol{\rho}) \right. \\ &\quad \left. + \begin{bmatrix} \tilde{\boldsymbol{B}} \\ \boldsymbol{0} \end{bmatrix}\boldsymbol{N_1}\boldsymbol{\Lambda K}(\boldsymbol{\rho})\right)\boldsymbol{\xi} + \left(\begin{bmatrix} \boldsymbol{B_0} \\ \boldsymbol{0} \end{bmatrix} + \begin{bmatrix} \tilde{\boldsymbol{B}} \\ \boldsymbol{0} \end{bmatrix}\boldsymbol{N_1}\right)\boldsymbol{w} + \boldsymbol{d}_{\boldsymbol{\xi}}. \end{aligned} \tag{24}$$

Denote

$$\begin{cases} \boldsymbol{\Lambda_{\max}} = \mathrm{diag}[\lambda_{1\max}\ \lambda_{2\max}\ \lambda_{3\max}] \\ \boldsymbol{\Lambda_{\min}} = \mathrm{diag}[\lambda_{1\min}\ \lambda_{2\min}\ \lambda_{3\min}] \\ \boldsymbol{\Lambda_{\mathrm{m}}} = (\boldsymbol{\Lambda}_{\max} + \boldsymbol{\Lambda}_{\min})/2 \end{cases} \tag{25}$$

with $\lambda_{*\max}$ and $\lambda_{*\min}$ being the maximal and minimal values of λ_*, respectively. So $\boldsymbol{\Lambda}$ can be written as

$$\boldsymbol{\Lambda} = \boldsymbol{\Lambda_m} + \boldsymbol{N_2}\tilde{\boldsymbol{\Lambda}} \tag{26}$$

where $\tilde{\boldsymbol{\Lambda}} = \boldsymbol{\Lambda_{max}} - \boldsymbol{\Lambda_m}$, $\boldsymbol{N_2}$ is a time-varying diagonal matrix and satisfies $|N_2| < 1$. With (26), we have

$$\begin{aligned}
&\begin{bmatrix} \boldsymbol{A_0}(\boldsymbol{\rho}) & \boldsymbol{0} \\ \boldsymbol{I} & \boldsymbol{0} \end{bmatrix} + \begin{bmatrix} \tilde{\boldsymbol{A}}(\boldsymbol{\rho}) \\ \boldsymbol{0} \end{bmatrix} \boldsymbol{N_1}\,[\boldsymbol{I}\ \boldsymbol{0}] + \begin{bmatrix} \boldsymbol{B_0} \\ \boldsymbol{0} \end{bmatrix} \boldsymbol{\Lambda K}(\boldsymbol{\rho}) + \begin{bmatrix} \tilde{\boldsymbol{B}} \\ \boldsymbol{0} \end{bmatrix} \boldsymbol{N_1 \Lambda K}(\boldsymbol{\rho}) \\
&= \begin{bmatrix} \boldsymbol{A_0}(\boldsymbol{\rho}) & \boldsymbol{0} \\ \boldsymbol{I} & \boldsymbol{0} \end{bmatrix} + \begin{bmatrix} \boldsymbol{B_0} \\ \boldsymbol{0} \end{bmatrix} \left(\boldsymbol{\Lambda_m} + \boldsymbol{N_2}\tilde{\boldsymbol{\Lambda}} \right) \boldsymbol{K}(\boldsymbol{\rho}) \\
&\quad + \begin{bmatrix} \tilde{\boldsymbol{A}}(\boldsymbol{\rho}) \\ \boldsymbol{0} \end{bmatrix} \boldsymbol{N_1}\,[\boldsymbol{I}\ \boldsymbol{0}] + \begin{bmatrix} \tilde{\boldsymbol{B}} \\ \boldsymbol{0} \end{bmatrix} \boldsymbol{N_1} \left(\boldsymbol{\Lambda_m} + \boldsymbol{N_2}\tilde{\boldsymbol{\Lambda}} \right) \boldsymbol{K}(\boldsymbol{\rho}) \\
&= \left(\begin{bmatrix} \boldsymbol{A_0}(\boldsymbol{\rho}) & \boldsymbol{0} \\ \boldsymbol{I} & \boldsymbol{0} \end{bmatrix} + \begin{bmatrix} \boldsymbol{B_0} \\ \boldsymbol{0} \end{bmatrix} \boldsymbol{\Lambda_m K}(\boldsymbol{\rho}) \right) + \begin{bmatrix} \tilde{\boldsymbol{A}}(\boldsymbol{\rho}) \\ \boldsymbol{0} \end{bmatrix} \boldsymbol{N_1}\,[\boldsymbol{I}\ \boldsymbol{0}] \\
&\quad + \begin{bmatrix} \tilde{\boldsymbol{B}} \\ \boldsymbol{0} \end{bmatrix} \boldsymbol{N_1 \Lambda_m K}(\boldsymbol{\rho}) + \begin{bmatrix} \boldsymbol{B_0} \\ \boldsymbol{0} \end{bmatrix} \boldsymbol{N_2}\tilde{\boldsymbol{\Lambda}}\boldsymbol{K}\,(\boldsymbol{\rho}) + \begin{bmatrix} \tilde{\boldsymbol{B}} \\ \boldsymbol{0} \end{bmatrix} \boldsymbol{N_3}\tilde{\boldsymbol{\Lambda}}\boldsymbol{K}(\boldsymbol{\rho})
\end{aligned}$$

with $\boldsymbol{N_3} = \boldsymbol{N_1 N_2}$. From the previous equation, the closed-loop system can be rewritten as

$$\dot{\boldsymbol{\xi}} = \boldsymbol{A}_{\boldsymbol{\xi c}}(\boldsymbol{\rho})\boldsymbol{\xi} + \boldsymbol{B}_{\boldsymbol{\xi c}}\boldsymbol{w} + \boldsymbol{d}_{\boldsymbol{\xi}} \tag{27}$$

where

$$\begin{cases} \boldsymbol{A}_{\boldsymbol{\xi c}}(\boldsymbol{\rho}) = \boldsymbol{A}_{\boldsymbol{\Xi}}(\boldsymbol{\rho}) + \tilde{\boldsymbol{A}}_{\mathbf{ext}}(\boldsymbol{\rho})\boldsymbol{N_1}\,[\boldsymbol{I}\ \ \boldsymbol{0}] + \tilde{\boldsymbol{B}}_{\mathbf{ext}}\boldsymbol{N_1 \Lambda_m K}(\boldsymbol{\rho}) \\ \qquad\qquad + \boldsymbol{B}_{\mathbf{ext}}\boldsymbol{N_2}\tilde{\boldsymbol{\Lambda}}\boldsymbol{K}\,(\boldsymbol{\rho}) + \tilde{\boldsymbol{B}}_{\mathbf{ext}}\boldsymbol{N_3}\tilde{\boldsymbol{\Lambda}}\boldsymbol{K}(\boldsymbol{\rho}) \\ \boldsymbol{B}_{\boldsymbol{\xi c}} = \boldsymbol{B}_{\mathbf{ext}} + \tilde{\boldsymbol{B}}_{\mathbf{ext}}\boldsymbol{N_1} \end{cases} \tag{28}$$

with

$$\begin{aligned}
\boldsymbol{A}_{\boldsymbol{\Xi}}(\boldsymbol{\rho}) &= \begin{bmatrix} \boldsymbol{A_0}(\boldsymbol{\rho}) & \boldsymbol{0} \\ \boldsymbol{I} & \boldsymbol{0} \end{bmatrix} + \boldsymbol{B}_{\mathbf{ext}}\boldsymbol{\Lambda_m}\boldsymbol{K}(\boldsymbol{\rho}) \\
\tilde{\boldsymbol{A}}_{\mathbf{ext}}(\boldsymbol{\rho}) &= \begin{bmatrix} \tilde{\boldsymbol{A}}(\boldsymbol{\rho}) \\ \boldsymbol{0} \end{bmatrix}, \quad \tilde{\boldsymbol{B}}_{\mathbf{ext}} = \begin{bmatrix} \tilde{\boldsymbol{B}} \\ \boldsymbol{0} \end{bmatrix}, \quad \boldsymbol{B}_{\mathbf{ext}} = \begin{bmatrix} \boldsymbol{B_0} \\ \boldsymbol{0} \end{bmatrix}.
\end{aligned}$$

In the tracking control problem, it is required that the tracking error can converge as soon as possible. Meanwhile, the control action should not be too large to avoid possible control effort saturation. Inspired by the LQR control, we propose the following cost function:

$$J = \int_0^\infty \left((\boldsymbol{C}\ \boldsymbol{\xi})^{\boldsymbol{T}}\boldsymbol{Q}\,(\boldsymbol{C\xi}) + \boldsymbol{u}^{\boldsymbol{T}}\boldsymbol{R}\boldsymbol{u} \right) dt \tag{29}$$

where $\boldsymbol{Q}$ and $\boldsymbol{R}$ are two positive definite matrices and $\boldsymbol{C} = [\boldsymbol{0}\ \ \boldsymbol{I}]$. The matrix $\boldsymbol{C}$ is used to select the integration of the tracking error in the augmented state vector. Note that Jcan be rewritten as

$$J = \int_0^\infty \left(\left(\boldsymbol{Q}^{\frac{1}{2}}\boldsymbol{C\xi} \right)^{\boldsymbol{T}} \left(\boldsymbol{Q}^{\frac{1}{2}}\boldsymbol{C\xi} \right) + \left(\boldsymbol{R}^{\frac{1}{2}}\boldsymbol{u} \right)^{\boldsymbol{T}} \left(\boldsymbol{R}^{\frac{1}{2}}\boldsymbol{u} \right) \right) dt. \tag{30}$$

Defining the controlled outputs as

$$\boldsymbol{z} = \begin{bmatrix} \boldsymbol{Q}^{\frac{1}{2}}\boldsymbol{C} \\ \boldsymbol{0} \end{bmatrix} \boldsymbol{\xi} + \begin{bmatrix} \boldsymbol{0} \\ \boldsymbol{R}^{\frac{1}{2}} \end{bmatrix} \boldsymbol{u} \tag{31}$$

we have

$$\begin{aligned}
\boldsymbol{z}^{\boldsymbol{T}}\boldsymbol{z} &= \left[\begin{bmatrix} \boldsymbol{Q}^{\frac{1}{2}}\boldsymbol{C} \\ \boldsymbol{0} \end{bmatrix} \boldsymbol{\xi} + \begin{bmatrix} \boldsymbol{0} \\ \boldsymbol{R}^{\frac{1}{2}} \end{bmatrix} \boldsymbol{u} \right]^{\boldsymbol{T}} \left[\begin{bmatrix} \boldsymbol{Q}^{\frac{1}{2}}\boldsymbol{C} \\ \boldsymbol{0} \end{bmatrix} \boldsymbol{\xi} + \begin{bmatrix} \boldsymbol{0} \\ \boldsymbol{R}^{\frac{1}{2}} \end{bmatrix} \boldsymbol{u} \right] \\
&= \boldsymbol{\xi}^{\boldsymbol{T}} \begin{bmatrix} \boldsymbol{Q}^{\frac{1}{2}}\boldsymbol{C} \\ \boldsymbol{0} \end{bmatrix}^{\boldsymbol{T}} \begin{bmatrix} \boldsymbol{Q}^{\frac{1}{2}}\boldsymbol{C} \\ \boldsymbol{0} \end{bmatrix} \boldsymbol{\xi} + \boldsymbol{u}^{\boldsymbol{T}} \begin{bmatrix} \boldsymbol{0} \\ \boldsymbol{R}^{\frac{1}{2}} \end{bmatrix}^{\boldsymbol{T}} \begin{bmatrix} \boldsymbol{0} \\ \boldsymbol{R}^{\frac{1}{2}} \end{bmatrix} \boldsymbol{u} \\
&= \left(\boldsymbol{Q}^{\frac{1}{2}}\boldsymbol{C\xi} \right)^{\boldsymbol{T}} \left(\boldsymbol{Q}^{\frac{1}{2}}\boldsymbol{C\xi} \right) + \left(\boldsymbol{R}^{\frac{1}{2}}\boldsymbol{u} \right)^{\boldsymbol{T}} \left(\boldsymbol{R}^{\frac{1}{2}}\boldsymbol{u} \right).
\end{aligned} \tag{32}$$

Note that J is the square of $||z||_2$. The optimization on the cost function J is reduced to the optimization on the two-norm of the controlled output. So the closed-loop system can be written as

$$\begin{cases} \dot{\boldsymbol{\xi}} = \boldsymbol{A}_{\boldsymbol{\xi c}}(\boldsymbol{\rho})\boldsymbol{\xi} + \boldsymbol{B}_{\boldsymbol{\xi c}}\boldsymbol{w} + \boldsymbol{d}_{\boldsymbol{\xi}} \\ \boldsymbol{z} = \boldsymbol{C}_{\boldsymbol{\xi c}}\boldsymbol{\xi} \end{cases} \tag{33}$$

where $\boldsymbol{C}_{\boldsymbol{\xi c}} = \overline{\boldsymbol{C}} + \overline{\boldsymbol{D}}\boldsymbol{K}$, with

$$\overline{\boldsymbol{C}} = \begin{bmatrix} \boldsymbol{Q}^{\frac{1}{2}}\boldsymbol{C} \\ \boldsymbol{0} \end{bmatrix}, \quad \overline{\boldsymbol{D}} = \begin{bmatrix} \boldsymbol{0} \\ \boldsymbol{R}^{\frac{1}{2}} \end{bmatrix}.$$

Note that there are two disturbance terms $\boldsymbol{w}$ and $\boldsymbol{d_\xi}$ involved in (33). Since these two disturbances are different in physical meaning, they are not treated equally here. To attenuate the effects of these two disturbances to the controlled outputs, we choose the following indexes:

$$\begin{cases} \|z\|_2 < \gamma_1 \|\boldsymbol{w}\|_2 \\ \|z\|_2 < \gamma_2 \left\|\boldsymbol{d}_{\boldsymbol{\xi}}\right\|_2. \end{cases} \tag{34}$$

With the above indexes, the control objective is to design a gain scheduling feedback controller such that, under zero-initial conditions, the indexes are satisfied.

Remark 6: The proposed control strategy for the system (22) is a state-feedback control. As the new-defined state $\boldsymbol{\xi}$ is a combination of the tracking error $\boldsymbol{e} = \boldsymbol{x} - \boldsymbol{r}$ and the error integral, the control law in (23) can be extended as

$$\boldsymbol{u} = \boldsymbol{K}_1(\boldsymbol{\rho})\boldsymbol{e} + \boldsymbol{K}_2(\boldsymbol{\rho}) \int_0^t \boldsymbol{e} d\tau.$$

It can be seen that the first term is a proportional control for the system in (21) and the second term is an integral control, which can be used to eliminate the tracking error. Therefore, the control law in (23) is a generalized proportional-integral control for the system in (21). Compared with the traditional proportional-integral-derivative (PID) controllers in [24]–[26], this formulation method can avoid the NP-hard problem in the controller design. The cost function in this paper is chosen as a linear quadratic form in which there are two positive-definite matrices. Since there are disturbance terms in (27), the cost function equals to the two-norm of the controlled output.

To deal with the uncertainties and external disturbances, we first introduce the following two lemmas.

Lemma 1 [27]: Given two positive constants γ_1 and γ_2, considering the closed-loop system in (33), a gain-scheduling state-feedback controller exists such as the (extended) bounded real lemma condition holds for some L_2-performance level $\gamma_1$and γ_2, if and only if there exists a symmetric positive definite matrix $\boldsymbol{P}$ satisfying the following conditions:

$$\begin{bmatrix} \boldsymbol{A}_{\boldsymbol{\xi c}}^{\boldsymbol{T}}(\boldsymbol{\rho})\boldsymbol{P} + \boldsymbol{P}\boldsymbol{A}_{\boldsymbol{\xi c}}(\boldsymbol{\rho}) & \boldsymbol{P}\boldsymbol{B}_{\boldsymbol{\xi c}} & \boldsymbol{C}_{\boldsymbol{\xi c}}^{\boldsymbol{T}} \\ * & -\boldsymbol{\gamma_1^2 I} & \boldsymbol{0} \\ * & * & -\boldsymbol{I} \end{bmatrix} < \boldsymbol{0} \tag{35}$$

$$\begin{bmatrix} \boldsymbol{A}_{\boldsymbol{\xi c}}^{\boldsymbol{T}}(\boldsymbol{\rho})\boldsymbol{P} + \boldsymbol{P}\boldsymbol{A}_{\boldsymbol{\xi c}}(\boldsymbol{\rho}) & \boldsymbol{P} & \boldsymbol{C}_{\boldsymbol{\xi c}}^{\boldsymbol{T}} \\ * & -\boldsymbol{\gamma_2^2 I} & \boldsymbol{0} \\ * & * & -\boldsymbol{I} \end{bmatrix} < \boldsymbol{0}. \tag{36}$$

Lemma 2 [28]: Let $\boldsymbol{\Theta} = \boldsymbol{\Theta}^{\boldsymbol{T}}$, $\overline{\boldsymbol{L}}$ and $\overline{\boldsymbol{E}}$ be real matrices with compatible dimensions, and $\overline{\boldsymbol{N}}^{\boldsymbol{T}}(t)$ be time-varying and satisfy $\overline{\boldsymbol{N}}^{\boldsymbol{T}}(t)\overline{\boldsymbol{N}}(t) < \boldsymbol{I}$, then the following condition:

$$\boldsymbol{\Theta} + \overline{\boldsymbol{L}}\,\overline{\boldsymbol{N}}(t)\overline{\boldsymbol{E}} + \overline{\boldsymbol{E}}^{\boldsymbol{T}}\overline{\boldsymbol{N}}^{\boldsymbol{T}}(t)\overline{\boldsymbol{L}}^{\boldsymbol{T}} < \boldsymbol{0} \tag{37}$$

holds if and only if there exists a positive scalar $\varepsilon > 0$ such that

$$\begin{bmatrix} \boldsymbol{\Theta} & \varepsilon\overline{\boldsymbol{L}} & \overline{\boldsymbol{E}}^{\boldsymbol{T}} \\ * & -\varepsilon\boldsymbol{I} & \boldsymbol{0} \\ * & * & -\varepsilon\boldsymbol{I} \end{bmatrix} < \boldsymbol{0} \tag{38}$$

is satisfied.

It is necessary to mention that the eigenvalues of the closed-loop system have a significant effect on the transient response. Also, the control inputs need to be restricted due to the physical limitations on the actuators. To constrain the eigenvalues of the closed-loop system to have a good transient response with relatively less control energy, we introduce the following lemma and definition.

Definition 1 (LMI Regions) [29]: A subset $\boldsymbol{D}$ of the complex plane is called an LMI region if there exist matrices $L_1 = L_1^T$ and L_2 such that

$$\boldsymbol{D} = \{z \in \boldsymbol{C} : f_{\boldsymbol{D}}(z) < \boldsymbol{0}\} \tag{39}$$

with

$$f_{\boldsymbol{D}}(z) := L_1 + zL_2 + \overline{z}L_2^T. \tag{40}$$

From the application aspect, some typical LMI regions are summarized as follows.

1) Half-plane $Re(z) < -\alpha : f_{\boldsymbol{D}}(z) := 2\alpha + z + \overline{z} < 0$.
2) Disk centered at $(-q, 0)$ with radius r

$$f_{\boldsymbol{D}}(z) := \begin{bmatrix} -r & q+z \\ q+\overline{z} & -r \end{bmatrix} < 0.$$

Lemma 3 [29]: The matrix $\boldsymbol{A}_{\boldsymbol{\xi c}}(\boldsymbol{\rho})$ is $\boldsymbol{D}$-stable if and only if there exists a symmetric matrix $\boldsymbol{P}$ such that

$$\boldsymbol{M}_{\boldsymbol{D}}(\boldsymbol{A}_{\boldsymbol{\xi c}}(\boldsymbol{\rho}), \boldsymbol{P}) < \boldsymbol{0},\ \boldsymbol{P} > \boldsymbol{0} \tag{41}$$

$$\begin{bmatrix}
\boldsymbol{\Xi}_Q & \boldsymbol{B}_{\mathbf{ext}} & \boldsymbol{Q}\boldsymbol{C}_{\boldsymbol{\xi}\mathbf{c}}^{\boldsymbol{T}} & \varepsilon_1(\boldsymbol{\rho})\tilde{\boldsymbol{B}}_{\mathbf{ext}} & \varepsilon_2(\boldsymbol{\rho})\tilde{\boldsymbol{B}}_{\mathbf{ext}} & \boldsymbol{H}^T\tilde{\boldsymbol{\Lambda}} & \boldsymbol{0} & \varepsilon_3(\boldsymbol{\rho})\tilde{\boldsymbol{B}}_{\mathbf{ext}} & \boldsymbol{H}^T\tilde{\boldsymbol{\Lambda}} & \varepsilon_4(\boldsymbol{\rho})\tilde{\boldsymbol{B}}_{\mathbf{ext}} & \boldsymbol{H}^T\boldsymbol{\Lambda}_m & \varepsilon_5(\boldsymbol{\rho})\tilde{\boldsymbol{A}}_{\mathbf{ext}} & \boldsymbol{Q}\boldsymbol{I}_{\mathbf{ext}} \\
* & -\gamma_1^2\boldsymbol{I} & \boldsymbol{0} & \boldsymbol{0} & \boldsymbol{0} & \boldsymbol{0} & \varepsilon_2(\boldsymbol{\rho})\boldsymbol{I} & \boldsymbol{0} & \boldsymbol{0} & \boldsymbol{0} & \boldsymbol{0} & \boldsymbol{0} & \boldsymbol{0} \\
* & * & \boldsymbol{I} & \boldsymbol{0} & \boldsymbol{0} & \boldsymbol{0} & \boldsymbol{0} & \boldsymbol{0} & \boldsymbol{0} & \boldsymbol{0} & \boldsymbol{0} & \boldsymbol{0} & \boldsymbol{0} \\
* & * & * & -\varepsilon_1(\boldsymbol{\rho})\boldsymbol{I} & \boldsymbol{0} & \boldsymbol{0} & \boldsymbol{0} & \boldsymbol{0} & \boldsymbol{0} & \boldsymbol{0} & \boldsymbol{0} & \boldsymbol{0} & \boldsymbol{0} \\
* & * & * & * & -\varepsilon_2(\boldsymbol{\rho})\boldsymbol{I} & \boldsymbol{0} & \boldsymbol{0} & \boldsymbol{0} & \boldsymbol{0} & \boldsymbol{0} & \boldsymbol{0} & \boldsymbol{0} & \boldsymbol{0} \\
* & * & * & * & * & -\varepsilon_1(\boldsymbol{\rho})\boldsymbol{I} & \boldsymbol{0} & \boldsymbol{0} & \boldsymbol{0} & \boldsymbol{0} & \boldsymbol{0} & \boldsymbol{0} & \boldsymbol{0} \\
* & * & * & * & * & * & -\varepsilon_2(\boldsymbol{\rho}) & \boldsymbol{0} & \boldsymbol{0} & \boldsymbol{0} & \boldsymbol{0} & \boldsymbol{0} & \boldsymbol{0} \\
* & * & * & * & * & * & * & -\varepsilon_3(\boldsymbol{\rho}) & \boldsymbol{0} & \boldsymbol{0} & \boldsymbol{0} & \boldsymbol{0} & \boldsymbol{0} \\
* & * & * & * & * & * & * & * & -\varepsilon_3(\boldsymbol{\rho})\boldsymbol{I} & \boldsymbol{0} & \boldsymbol{0} & \boldsymbol{0} & \boldsymbol{0} \\
* & * & * & * & * & * & * & * & * & -\varepsilon_4(\boldsymbol{\rho})\boldsymbol{I} & \boldsymbol{0} & \boldsymbol{0} & \boldsymbol{0} \\
* & * & * & * & * & * & * & * & * & * & -\varepsilon_4(\boldsymbol{\rho})\boldsymbol{I} & \boldsymbol{0} & \boldsymbol{0} \\
* & * & * & * & * & * & * & * & * & * & * & -\varepsilon_5(\boldsymbol{\rho})\boldsymbol{I} & \boldsymbol{0} \\
* & * & * & * & * & * & * & * & * & * & * & * & -\varepsilon_5(\boldsymbol{\rho})\boldsymbol{I}
\end{bmatrix} \tag{43}$$

$$\begin{bmatrix}
\boldsymbol{\Xi}_Q & \boldsymbol{I} & \boldsymbol{Q}\boldsymbol{C}_{\boldsymbol{\xi}\mathbf{c}}^{\boldsymbol{T}} & \varepsilon_6(\boldsymbol{\rho})\tilde{\boldsymbol{B}}_{\mathbf{ext}} & \boldsymbol{H}^T\tilde{\boldsymbol{\Lambda}} & \varepsilon_7(\boldsymbol{\rho})\tilde{\boldsymbol{B}}_{\mathbf{ext}} & \boldsymbol{H}^T\tilde{\boldsymbol{\Lambda}} & \varepsilon_8(\boldsymbol{\rho})\tilde{\boldsymbol{B}}_{\mathbf{ext}} & \boldsymbol{H}^T\boldsymbol{\Lambda}_m & \varepsilon_9(\boldsymbol{\rho})\tilde{\boldsymbol{A}}_{\mathbf{ext}} & \boldsymbol{Q}\boldsymbol{I}_{\mathbf{ext}} \\
* & -\gamma_2^2\boldsymbol{I} & \boldsymbol{0} & \boldsymbol{0} & \boldsymbol{0} & \boldsymbol{0} & \boldsymbol{0} & \boldsymbol{0} & \boldsymbol{0} & \boldsymbol{0} & \boldsymbol{0} \\
* & * & \boldsymbol{I} & \boldsymbol{0} & \boldsymbol{0} & \boldsymbol{0} & \boldsymbol{0} & \boldsymbol{0} & \boldsymbol{0} & \boldsymbol{0} & \boldsymbol{0} \\
* & * & * & -\varepsilon_6(\boldsymbol{\rho})\boldsymbol{I} & \boldsymbol{0} & \boldsymbol{0} & \boldsymbol{0} & \boldsymbol{0} & \boldsymbol{0} & \boldsymbol{0} & \boldsymbol{0} \\
* & * & * & * & -\varepsilon_6(\boldsymbol{\rho})\boldsymbol{I} & \boldsymbol{0} & \boldsymbol{0} & \boldsymbol{0} & \boldsymbol{0} & \boldsymbol{0} & \boldsymbol{0} \\
* & * & * & * & * & -\varepsilon_7(\boldsymbol{\rho})\boldsymbol{I} & \boldsymbol{0} & \boldsymbol{0} & \boldsymbol{0} & \boldsymbol{0} & \boldsymbol{0} \\
* & * & * & * & * & * & -\varepsilon_7(\boldsymbol{\rho})\boldsymbol{I} & \boldsymbol{0} & \boldsymbol{0} & \boldsymbol{0} & \boldsymbol{0} \\
* & * & * & * & * & * & * & -\varepsilon_8(\boldsymbol{\rho})\boldsymbol{I} & \boldsymbol{0} & \boldsymbol{0} & \boldsymbol{0} \\
* & * & * & * & * & * & * & * & -\varepsilon_8(\boldsymbol{\rho})\boldsymbol{I} & \boldsymbol{0} & \boldsymbol{0} \\
* & * & * & * & * & * & * & * & * & -\varepsilon_9(\boldsymbol{\rho})\boldsymbol{I} & \boldsymbol{0} \\
* & * & * & * & * & * & * & * & * & * & -\varepsilon_9(\boldsymbol{\rho})\boldsymbol{I}
\end{bmatrix} \tag{44}$$

$$\begin{bmatrix}
-r\,\boldsymbol{Q} & q\,\boldsymbol{Q} + \boldsymbol{A}_{\boldsymbol{\Xi}}(\boldsymbol{\rho})\,\boldsymbol{Q} & \varepsilon_{10}(\boldsymbol{\rho})\tilde{\boldsymbol{B}}_{\mathbf{ext}} & \boldsymbol{0} & \varepsilon_{11}(\boldsymbol{\rho})\boldsymbol{B}_{\mathbf{ext}} & \boldsymbol{0} & \varepsilon_{12}(\boldsymbol{\rho})\tilde{\boldsymbol{B}}_{\mathbf{ext}} & \boldsymbol{0} & \varepsilon_{13}(\boldsymbol{\rho})\tilde{\boldsymbol{A}}_{\mathbf{ext}}(\boldsymbol{\rho}) & \boldsymbol{0} \\
* & -r\,\boldsymbol{Q} & \boldsymbol{0} & \boldsymbol{H}^T\tilde{\boldsymbol{\Lambda}} & \boldsymbol{0} & \boldsymbol{H}^T\tilde{\boldsymbol{\Lambda}} & \boldsymbol{0} & \boldsymbol{H}^T\boldsymbol{\Lambda}_{\mathbf{m}} & \boldsymbol{0} & \boldsymbol{Q}\boldsymbol{I}_{\mathbf{ext}} \\
* & * & -\varepsilon_{10}(\boldsymbol{\rho})\boldsymbol{I} & \boldsymbol{0} & \boldsymbol{0} & \boldsymbol{0} & \boldsymbol{0} & \boldsymbol{0} & \boldsymbol{0} & \boldsymbol{0} \\
* & * & * & -\varepsilon_{10}(\boldsymbol{\rho})\boldsymbol{I} & \boldsymbol{0} & \boldsymbol{0} & \boldsymbol{0} & \boldsymbol{0} & \boldsymbol{0} & \boldsymbol{0} \\
* & * & * & * & -\varepsilon_{11}(\boldsymbol{\rho})\boldsymbol{I} & \boldsymbol{0} & \boldsymbol{0} & \boldsymbol{0} & \boldsymbol{0} & \boldsymbol{0} \\
* & * & * & * & * & -\varepsilon_{11}(\boldsymbol{\rho})\boldsymbol{I} & \boldsymbol{0} & \boldsymbol{0} & \boldsymbol{0} & \boldsymbol{0} \\
* & * & * & * & * & * & -\varepsilon_{12}(\boldsymbol{\rho})\boldsymbol{I} & \boldsymbol{0} & \boldsymbol{0} & \boldsymbol{0} \\
* & * & * & * & * & * & * & -\varepsilon_{12}(\boldsymbol{\rho})\boldsymbol{I} & \boldsymbol{0} & \boldsymbol{0} \\
* & * & * & * & * & * & * & * & -\varepsilon_{13}(\boldsymbol{\rho})\boldsymbol{I} & \boldsymbol{0} \\
* & * & * & * & * & * & * & * & * & -\varepsilon_{13}(\boldsymbol{\rho})\boldsymbol{I}
\end{bmatrix}. \tag{45}$$

where

$$\boldsymbol{M_D}\left(\boldsymbol{A_{\xi c}}(\boldsymbol{\rho}),P\right) = \boldsymbol{L_1}\otimes\boldsymbol{P}+\boldsymbol{L_2}\otimes\left(\boldsymbol{PA_{\xi c}}(\boldsymbol{\rho})\right)+\boldsymbol{L_2^T}\otimes\left(\boldsymbol{A_{\xi c}^T}(\boldsymbol{\rho})\boldsymbol{P}\right).$$

Now we are in the position to propose the gain-scheduling controller design method. Before introducing the following theorem, we denote:

$$\boldsymbol{\Xi}_Q = \boldsymbol{QA_\Xi^T}(\boldsymbol{\rho})+\boldsymbol{A_\Xi}(\boldsymbol{\rho})\boldsymbol{Q}. \tag{42}$$

Theorem 1: Considering the closed-loop system in (33), a gain-scheduling state-feedback controller exists such that the closed-loop system in (33) is $\boldsymbol{D}$-stable in the disk centered at $(-q,0)$ with a radius r and the H_∞ performance index in (34) holds, if and only if there exist $\varepsilon(\boldsymbol{\rho})$, $\boldsymbol{H}$, and a symmetric positive definite matrix $\boldsymbol{Q}$ satisfying the conditions (43)–(45) as shown at the bottom of the previous page. Moreover, $\boldsymbol{H}=\boldsymbol{KQ}$. Proof can be found in Appendix A.

For the vehicle system, the time-varying parameters can be assumed to be bounded as $\rho_l \in [\,\underline{\rho_l}\ \overline{\rho}_l\,]$ $(l=1,\ 2,\ 3)$, where the upper bounds $\overline{\rho}_l$ and the lower bounds $\underline{\rho_l}$ are determined by the bounds on V_x and Ω_z. As the system matrices $\boldsymbol{A_{\xi c}}(\boldsymbol{\rho})$ are linearly dependent on the defined time-varying parameters $\boldsymbol{\rho}$, $\boldsymbol{A_{\xi c}}(\boldsymbol{\rho})$ can be rewritten as

$$\boldsymbol{A_{\xi c}}(\boldsymbol{\rho}) = \sum_{i=1}^{8}\theta_i(\boldsymbol{\rho})\boldsymbol{A_{\xi ci}}(\omega_i) \tag{46}$$

where ω_i are the vertices of the polytope formed by all the extremities of each varying gain-scheduling parameter $\boldsymbol{\rho}$, and $\theta_i(\boldsymbol{\rho})$ are defined as

$$\theta_i(\boldsymbol{\rho}) = \frac{\prod_{l=1}^{3}\left|\rho_l-\Upsilon(\omega_i)_l\right|}{\prod_{l=1}^{3}\left|\overline{\rho}_l-\underline{\rho_l}\right|},\quad i=1,2,\ldots,8 \tag{47}$$

where $\theta_i(\boldsymbol{\rho})\geq 0$ and satisfy

$$\sum_{i=1}^{8}\theta_i(\boldsymbol{\rho}) = 1. \tag{48}$$

$$\boldsymbol{\Pi}_{1ij}=\begin{bmatrix}
\boldsymbol{\Xi}_{Qij} & \boldsymbol{B_{\mathrm{ext}i}} & \boldsymbol{QC_{\xi i\mathbf{c}}^T} & \varepsilon_{1i}(\boldsymbol{\rho})\tilde{\boldsymbol{B}}_{\mathbf{ext}j} & \varepsilon_2(\boldsymbol{\rho})\tilde{\boldsymbol{B}}_{\mathbf{ext}j} & \boldsymbol{H_i^T}\tilde{\boldsymbol{\Lambda}}_i & \boldsymbol{0} & \varepsilon_{3i}(\boldsymbol{\rho})\tilde{\boldsymbol{B}}_{\mathbf{ext}j} & \boldsymbol{H_i^T}\tilde{\boldsymbol{\Lambda}}_j & \varepsilon_{4i}(\boldsymbol{\rho})\tilde{\boldsymbol{B}}_{\mathbf{ext}j} & \boldsymbol{H_i^T}\boldsymbol{\Lambda}_{mj} & \varepsilon_{5i}(\boldsymbol{\rho})\tilde{\boldsymbol{A}}_{\mathbf{ext}j} & \boldsymbol{QI_{\mathrm{ext}}}\\
* & -\gamma_1^2\boldsymbol{I} & \boldsymbol{0} & \boldsymbol{0} & \boldsymbol{0} & \boldsymbol{0} & \varepsilon_2(\boldsymbol{\rho})\boldsymbol{I} & \boldsymbol{0} & \boldsymbol{0} & \boldsymbol{0} & \boldsymbol{0} & \boldsymbol{0} & \boldsymbol{0}\\
* & * & \boldsymbol{I} & \boldsymbol{0} & \boldsymbol{0} & \boldsymbol{0} & \boldsymbol{0} & \boldsymbol{0} & \boldsymbol{0} & \boldsymbol{0} & \boldsymbol{0} & \boldsymbol{0} & \boldsymbol{0}\\
* & * & * & -\varepsilon_{1i}(\boldsymbol{\rho})\boldsymbol{I} & \boldsymbol{0} & \boldsymbol{0} & \boldsymbol{0} & \boldsymbol{0} & \boldsymbol{0} & \boldsymbol{0} & \boldsymbol{0} & \boldsymbol{0} & \boldsymbol{0}\\
* & * & * & * & -\varepsilon_{2i}(\boldsymbol{\rho})\boldsymbol{I} & \boldsymbol{0} & \boldsymbol{0} & \boldsymbol{0} & \boldsymbol{0} & \boldsymbol{0} & \boldsymbol{0} & \boldsymbol{0} & \boldsymbol{0}\\
* & * & * & * & * & -\varepsilon_{1i}(\boldsymbol{\rho})\boldsymbol{I} & \boldsymbol{0} & \boldsymbol{0} & \boldsymbol{0} & \boldsymbol{0} & \boldsymbol{0} & \boldsymbol{0} & \boldsymbol{0}\\
* & * & * & * & * & * & -\varepsilon_{2i}(\boldsymbol{\rho}) & \boldsymbol{0} & \boldsymbol{0} & \boldsymbol{0} & \boldsymbol{0} & \boldsymbol{0} & \boldsymbol{0}\\
* & * & * & * & * & * & * & -\varepsilon_{3i}(\boldsymbol{\rho}) & \boldsymbol{0} & \boldsymbol{0} & \boldsymbol{0} & \boldsymbol{0} & \boldsymbol{0}\\
* & * & * & * & * & * & * & * & -\varepsilon_{3i}(\boldsymbol{\rho})\boldsymbol{I} & \boldsymbol{0} & \boldsymbol{0} & \boldsymbol{0} & \boldsymbol{0}\\
* & * & * & * & * & * & * & * & * & -\varepsilon_{4i}(\boldsymbol{\rho})\boldsymbol{I} & \boldsymbol{0} & \boldsymbol{0} & \boldsymbol{0}\\
* & * & * & * & * & * & * & * & * & * & -\varepsilon_{4i}(\boldsymbol{\rho})\boldsymbol{I} & \boldsymbol{0} & \boldsymbol{0}\\
* & * & * & * & * & * & * & * & * & * & * & -\varepsilon_{5i}(\boldsymbol{\rho})\boldsymbol{I} & \boldsymbol{0}\\
* & * & * & * & * & * & * & * & * & * & * & * & -\varepsilon_{5i}(\boldsymbol{\rho})\boldsymbol{I}
\end{bmatrix} < 0$$

$$\boldsymbol{\Pi}_{2ij}=\begin{bmatrix}
\boldsymbol{\Xi_{Qij}} & \boldsymbol{I} & \boldsymbol{QC_{\xi\mathbf{c}i}^T} & \varepsilon_{6i}(\boldsymbol{\rho})\tilde{\boldsymbol{B}}_{\mathbf{ext}j} & \boldsymbol{H_i^T}\tilde{\boldsymbol{\Lambda}}_j & \varepsilon_{7i}(\boldsymbol{\rho})\tilde{\boldsymbol{B}}_{\mathbf{ext}j} & \boldsymbol{H_i^T}\tilde{\boldsymbol{\Lambda}}_j & \varepsilon_{8i}(\boldsymbol{\rho})\tilde{\boldsymbol{B}}_{\mathbf{ext}j} & \boldsymbol{H_i^T}\boldsymbol{\Lambda}_{mj} & \varepsilon_{9i}(\boldsymbol{\rho})\tilde{\boldsymbol{A}}_{\mathbf{ext}j} & \boldsymbol{QI_{\mathrm{ext}}}\\
* & -\gamma_2^2\boldsymbol{I} & \boldsymbol{0} & \boldsymbol{0} & \boldsymbol{0} & \boldsymbol{0} & \boldsymbol{0} & \boldsymbol{0} & \boldsymbol{0} & \boldsymbol{0} & \boldsymbol{0}\\
* & * & \boldsymbol{I} & \boldsymbol{0} & \boldsymbol{0} & \boldsymbol{0} & \boldsymbol{0} & \boldsymbol{0} & \boldsymbol{0} & \boldsymbol{0} & \boldsymbol{0}\\
* & * & * & -\varepsilon_{6i}(\boldsymbol{\rho})\boldsymbol{I} & \boldsymbol{0} & \boldsymbol{0} & \boldsymbol{0} & \boldsymbol{0} & \boldsymbol{0} & \boldsymbol{0} & \boldsymbol{0}\\
* & * & * & * & -\varepsilon_{6i}(\boldsymbol{\rho})\boldsymbol{I} & \boldsymbol{0} & \boldsymbol{0} & \boldsymbol{0} & \boldsymbol{0} & \boldsymbol{0} & \boldsymbol{0}\\
* & * & * & * & * & -\varepsilon_{7i}(\boldsymbol{\rho})\boldsymbol{I} & \boldsymbol{0} & \boldsymbol{0} & \boldsymbol{0} & \boldsymbol{0} & \boldsymbol{0}\\
* & * & * & * & * & * & -\varepsilon_{7i}(\boldsymbol{\rho})\boldsymbol{I} & \boldsymbol{0} & \boldsymbol{0} & \boldsymbol{0} & \boldsymbol{0}\\
* & * & * & * & * & * & * & -\varepsilon_{8i}(\boldsymbol{\rho})\boldsymbol{I} & \boldsymbol{0} & \boldsymbol{0} & \boldsymbol{0}\\
* & * & * & * & * & * & * & * & -\varepsilon_{8i}(\boldsymbol{\rho})\boldsymbol{I} & \boldsymbol{0} & \boldsymbol{0}\\
* & * & * & * & * & * & * & * & * & -\varepsilon_{9i}(\boldsymbol{\rho})\boldsymbol{I} & \boldsymbol{0}\\
* & * & * & * & * & * & * & * & * & * & -\varepsilon_{9i}(\boldsymbol{\rho})\boldsymbol{I}
\end{bmatrix} < \boldsymbol{0}$$

$$\boldsymbol{\Pi}_{3ij}=\begin{bmatrix}
-r\boldsymbol{Q} & q\boldsymbol{Q}+\boldsymbol{A_{\Xi i}}(\boldsymbol{\rho})\boldsymbol{Q} & \varepsilon_{10i}(\boldsymbol{\rho})\tilde{\boldsymbol{B}}_{\mathbf{ext}i} & \boldsymbol{0} & \varepsilon_{11i}(\boldsymbol{\rho})\boldsymbol{B}_{\mathbf{ext}j} & \boldsymbol{0} & \varepsilon_{12i}(\boldsymbol{\rho})\tilde{\boldsymbol{B}}_{\mathbf{ext}j} & \boldsymbol{0} & \varepsilon_{13i}(\boldsymbol{\rho})\tilde{\boldsymbol{A}}_{\mathbf{ext}j}(\boldsymbol{\rho}) & \boldsymbol{0}\\
* & -r\boldsymbol{Q} & \boldsymbol{0} & \boldsymbol{H_i^T}\tilde{\boldsymbol{\Lambda}}_j & \boldsymbol{0} & \boldsymbol{H_i^T}\tilde{\boldsymbol{\Lambda}}_j & \boldsymbol{0} & \boldsymbol{H_i^T}\tilde{\boldsymbol{\Lambda}}_m & \boldsymbol{0} & \boldsymbol{QI_{\mathrm{ext}}}\\
* & * & -\varepsilon_{10i}(\boldsymbol{\rho})\boldsymbol{I} & \boldsymbol{0} & \boldsymbol{0} & \boldsymbol{0} & \boldsymbol{0} & \boldsymbol{0} & \boldsymbol{0} & \boldsymbol{0}\\
* & * & * & -\varepsilon_{10i}(\boldsymbol{\rho})\mathbf{I} & \boldsymbol{0} & \boldsymbol{0} & \boldsymbol{0} & \boldsymbol{0} & \boldsymbol{0} & \boldsymbol{0}\\
* & * & * & * & -\varepsilon_{11i}(\boldsymbol{\rho})\boldsymbol{I} & \boldsymbol{0} & \boldsymbol{0} & \boldsymbol{0} & \boldsymbol{0} & \boldsymbol{0}\\
* & * & * & * & * & -\varepsilon_{11i}(\boldsymbol{\rho})\boldsymbol{I} & \boldsymbol{0} & \boldsymbol{0} & \boldsymbol{0} & \boldsymbol{0}\\
* & * & * & * & * & * & -\varepsilon_{12i}(\boldsymbol{\rho})\boldsymbol{I} & \boldsymbol{0} & \boldsymbol{0} & \boldsymbol{0}\\
* & * & * & * & * & * & * & -\varepsilon_{12i}(\boldsymbol{\rho})\boldsymbol{I} & \boldsymbol{0} & \boldsymbol{0}\\
* & * & * & * & * & * & * & * & -\varepsilon_{13i}(\boldsymbol{\rho})\boldsymbol{I} & \boldsymbol{0}\\
* & * & * & * & * & * & * & * & * & -\varepsilon_{13i}(\boldsymbol{\rho})\boldsymbol{I}
\end{bmatrix} < \boldsymbol{0}$$

$\Upsilon(\omega_i)_l$ are defined as

$$\Upsilon(\omega_i)_l = \begin{cases} \overline{\rho}_l, & \text{if } (\omega_i)_l = \underline{\rho_l} \\ \underline{\rho_l}, & \text{otherwise.} \end{cases} \tag{49}$$

Theorem 2: Considering the closed-loop system in (33), a gain-scheduling state-feedback controller exists such that the closed-loop system in (33) is $\boldsymbol{D}$-stable in the disk centered at $(-q, 0)$ with radius r and the H_∞ performance index in (34) holds, if and only if there exist ε_i, $\boldsymbol{H}_i$, and a symmetric positive definite matrix $\boldsymbol{Q}$ such as the following matrix inequalities are feasible:

$$\begin{cases} \boldsymbol{\Pi}_{1ij} + \boldsymbol{\Pi}_{1ji} < \boldsymbol{0} \\ \boldsymbol{\Pi}_{2ij} + \boldsymbol{\Pi}_{2ji} < \boldsymbol{0} \\ \boldsymbol{\Pi}_{3ij} + \boldsymbol{\Pi}_{3ji} < \boldsymbol{0} \end{cases} \tag{50}$$

for $1 \le i \le j \le 8$. Here, $\boldsymbol{\Pi}_{1ij}$, $\boldsymbol{\Pi}_{2ij}$ and $\boldsymbol{\Pi}_{3ij}$ are shown at the bottom of the previous page. Moreover, $\boldsymbol{K_i} = \boldsymbol{H_i Q^{-1}}$. Proof can be found in Appendix B.

In the implementation, the final controller gain can be calculated as

$$\boldsymbol{K} = \sum_{i-1}^{8} \theta_i \boldsymbol{H_i}\, \boldsymbol{Q}^{-1}. \tag{51}$$

Note that in the previous equation, only the coefficients θ_i are computed on-line with (47), while $\boldsymbol{H_i}$ are solved offline using the information of the parameter bounds. Thus, the proposed FT controller has low on-line computational complexity and can be easily implemented. Also note that there are two performance indexes γ_1 and γ_2 in (34). A minimum γ_2 with a prescribed γ_1 can be obtained by using the following corollary.

Corollary 1: The minimum performance index γ_2 with a prescribed γ_1 in Theorem 2 can be found by solving the following convex optimization problem:

$$\min \gamma_2^2$$
$$\text{s.t. (50) holds for } 1 \le i \le j \le 8.$$

Remark 7: In Corollary 1, we only optimize γ_2 while constraining the γ_1 under a prescribed level. The prescribed value of γ_1 is manually chosen from a large value until a smallest one with which the LMIs in Theorem 2 are feasible, or chosen by checking the control performance. This technique is similar with the one in robust H_2/H_∞ control and filtering [36].

IV. Simulation Investigations

Three simulation cases based on a high-fidelity full-vehicle model constructed in CarSim® were conducted. The vehicle parameters in the simulations were taken from an actual prototype FWIA electric ground vehicle developed in the authors' group at The Ohio State University. Refer to [30] and [31] for the details of the test vehicle platform. In the simulation, we used $\mathbf{Q} = \boldsymbol{I}_{3\times 3}$ and $\boldsymbol{R} = 0.2\boldsymbol{I}_{3\times 3}$.

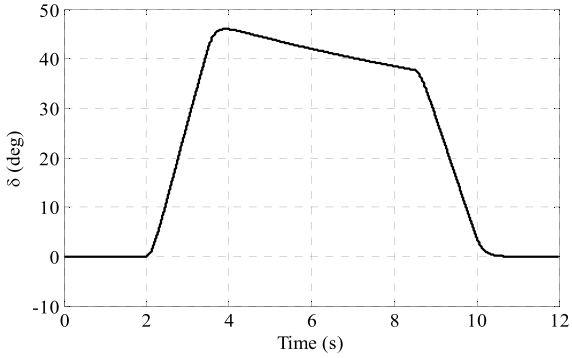

Fig. 3. Hand-wheel steering signal in the J-turn simulation.

A. Reference Signal Generations

Without appropriate accommodations, in-wheel motor or/and steering system faults may result in an unsatisfactory performance, and the vehicle will deviate from the desired trajectory quickly. The control objective is to control the vehicle to follow the desired trajectory even if some of the actuators are in fault. The reference model for the longitudinal speed can be written as [20]

$$V_{\mathrm{rx}} = V_{x0} + \int_{t_0}^{t} a_{\mathrm{rx}} dt \tag{52}$$

where V_{x0} is the initial vehicle speed at time t_0 and a_{rx} is the desired vehicle acceleration that can be calculated from the accelerator/brake pedal positions.

With the vehicle model (11), one can see that the vehicle lateral velocity and desired yaw rate can be simultaneously regulated with the external yaw moment generated with torque differences and the automatic steering using a steer-by-wire system. It is known that a zero vehicle lateral velocity can result in zero vehicle sideslip angle, and the vehicle sideslip angle should be contained to improve the vehicle stability [32], [33]. So the vehicle lateral velocity reference is chosen to be zero.

The desired vehicle yaw rate reference Ω_{rz} can be generated from the driver's steering angle and the vehicle states through reference models. The yaw rate reference can be calculated as [34]

$$\Omega_{\mathrm{rz}} = \frac{b_1 s + b_0}{a_2 s^2 + a_1 s + a_0} \delta(s) \tag{53}$$

where the parameters a_i and b_i are functions of the vehicle parameters and vehicle states, respectively [35], δ is the ground-wheel steering angle which can be calculated as $\delta = \delta_h / GR$, with GR being the gear ratio of the steering mechanism linkage, and δ_h is the hand-wheel steering angle. The GR value in the simulations is 10.

B. J-Turn Simulation

The vehicle ran at a low speed range in this simulation. The desired speed increased from 9 to 13 m/s in 8 s. A counterclockwise turn was introduced with the handwheel steering angle shown in Fig. 3. Three different faults were sequentially applied in this test: at 4 s, a loss-of-effectiveness fault occurred

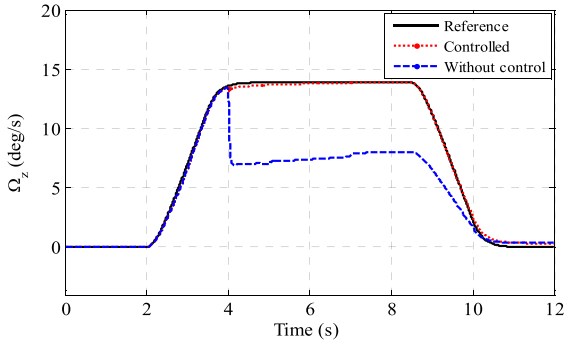

Fig. 4. Vehicle yaw rates in the J-turn simulation.

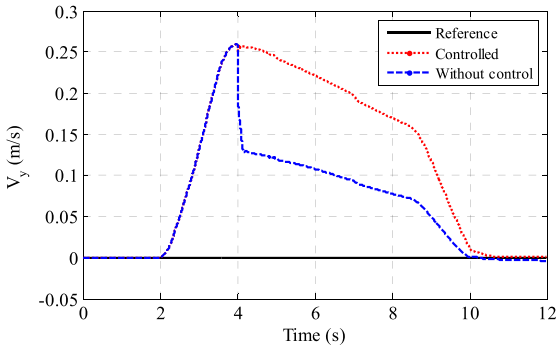

Fig. 6. Vehicle lateral speeds in the J-turn simulation.

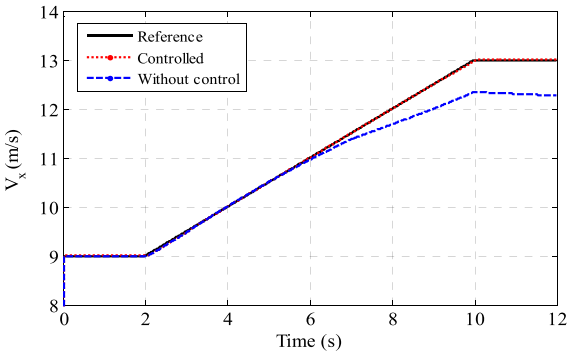

Fig. 5. Vehicle longitudinal speeds in the J-turn simulation.

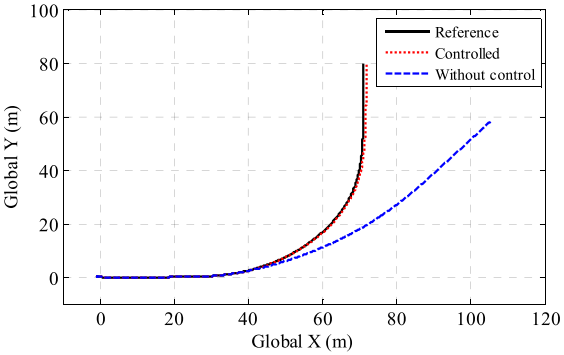

Fig. 7. Comparison of the vehicle trajectories in the J-turn simulation.

to the steering system and made the control effectiveness of the steering system decrease to half of its desired value, that is, $\delta = 0.5\delta_d$; at 5 s, an additive fault occurred to the front-right in-wheel motor, which made the motor torque changed to $T_{\rm fr} = T_{dfr} + \Delta T_{\rm fr}$ with $T_{\rm dfr}$ being the desired torque and $\Delta T_{\rm fr} = -20 - 10\sin(t)$; and at 7 s, a loss-of-effectiveness fault occurred to the rear-left in-wheel motor, which made the actual motor torque decrease to half of its desired value. To better show the performance of the proposed FT controller, the states of an uncontrolled vehicle with the same handwheel steering input and motor torque control signals are also plotted in the figures.

Fig. 4 shows the vehicle yaw rate under the proposed FT controller. One can see that the yaw rate of the controlled vehicle under the FT controller was very close to the reference, whereas the yaw rate of the uncontrolled vehicle deviated from the desired value as soon as the faults were introduced. Vehicle longitudinal speeds are plotted in Fig. 5, from which one can see that the longitudinal speed tracking error of the uncontrolled vehicle started to increase at 5 s. This is because the additive fault which changed the in-wheel motor torque was introduced at this time, whereas for the controlled vehicle, the longitudinal speed can track the reference well. The similar conclusion can be made to the lateral speed control result which is plotted in Fig. 6. Note that the lateral speed of the uncontrolled vehicle is smaller than that of the controlled one. This is because the uncontrolled vehicle could not make the turn as desired due to the actuator faults. The vehicle global trajectories are compared in Fig. 7, where we can see that even though three different faults were introduced, the vehicle could still track the reference well.

It is necessary to mention that the steering system fault in this simulation was modeled by $\delta = 0.5\delta_d$, which means that if the steering system has a hardware redundancy, for example, the dual-motor architecture, the fault model $\delta = 0.5\delta_d$ can describe the case where one of the steering motors is in a total failure. Note that if both of the steering motors fail, the steering torque will become zero and will not contribute to the control authority.

C. Single-Lane Change

In this simulation, the vehicle was controlled to make a single-lane change at a high speed. Both the steering and in-wheel motor faults were applied as follows: at 3 s an additive fault and a loss-of-effectiveness fault were applied to the steering system. These two faults made the actual ground-wheel steering angle change to $\delta = 0.6\delta_d - 3\,\text{deg}$; at 6 s an in-wheel fault which made the motor torque stuck at $-$ 20 N.m was introduced to the rear-left in-wheel motor.

The hand-wheel steering angle is shown in Fig 8. The yaw rate control results are plotted in Fig. 9, from which one can see that the yaw rate of the controlled faulty vehicle could always follow the reference, whereas the yaw rate of the uncontrolled faulty vehicle jumped and deviated from the reference at 3 s, because of the two faults applied to the

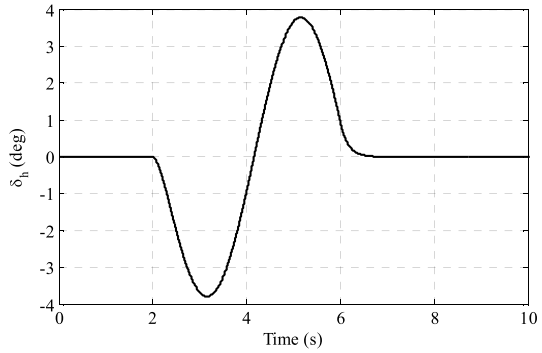

Fig. 8. Steering wheel signal in the single-lane change simulation.

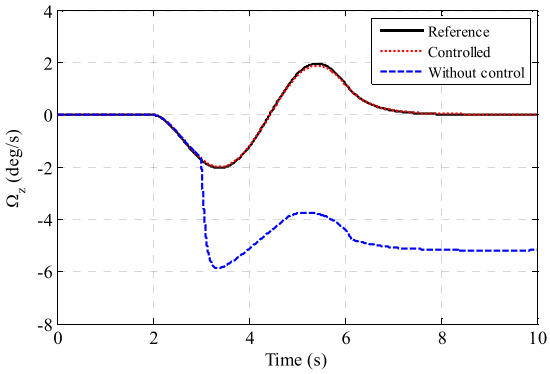

Fig. 9. Vehicle yaw rates in the single-lane change simulation.

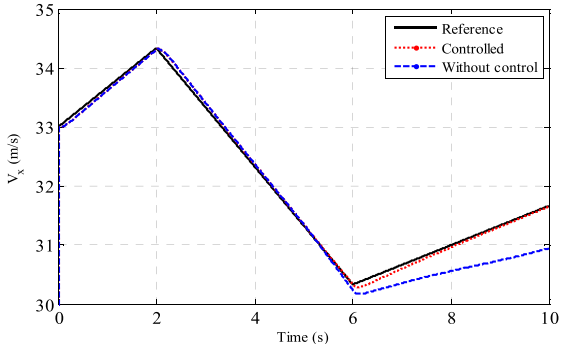

Fig. 10. Vehicle longitudinal speeds in the single-lane change simulation.

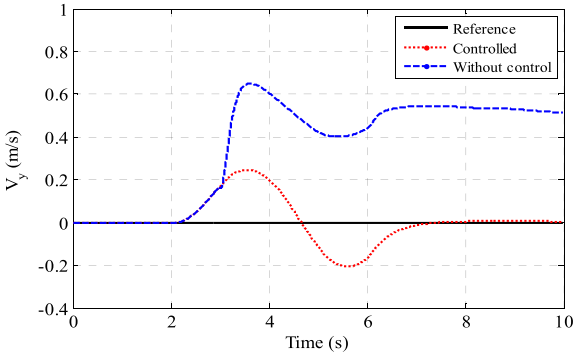

Fig. 11. Vehicle lateral speeds in the single-lane change simulation.

steering system. The vehicle longitudinal and lateral speeds shown in Figs. 10 and 11, respectively. One can see from these

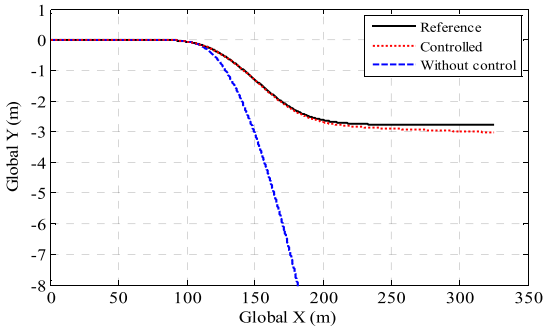

Fig. 12. Comparison of the vehicle trajectories in the single-lane change simulation.

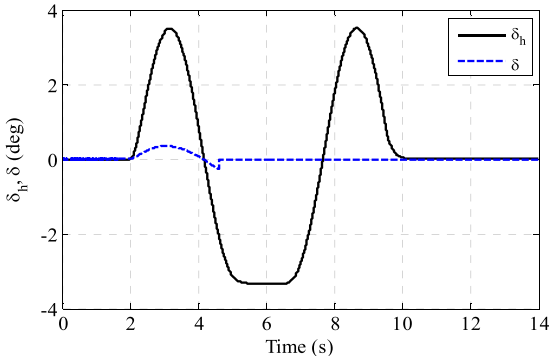

Fig. 13. Steering wheel angle and ground-wheel angle in the double-lane change simulation.

two figures that both of the speeds could be well controlled. For the uncontrolled vehicle, however, the vehicle speeds started to deviate from the desired values as soon as the faults were introduced. The vehicle global trajectories are shown in Fig. 12. One can observe again that the proposed FT controller ensured the vehicle tracking performance no matter which kind of fault was applied.

D. Double-Lane Change

In the previous simulations, we investigated the performance of the FT controller in the cases where the steering system partially lost its control effectiveness. In this simulation, the control performance of the FT controller in the case where the steering system totally failed is investigated. The failure of the steering system may result from many reasons such as broken wires, breakdown of the steering motors, and so on. If the steering system failure occurs, the steering actuator floats with zero moment and does not contribute to the control authority. Thanks to the FWIA vehicle architecture, the vehicle yaw rate may still be regulated with the external yaw moment generated by the torque difference between the left and right motors.

The hand-wheel steering angle and the vehicle's actual ground-wheel steering angle are shown in Fig. 13. The ground-wheel steering angle changed to zero at 4.5 s due to the steering system failure. The vehicle yaw rate is shown in Fig. 14, where we can observe that the yaw rate tracking error in this case was greater than these in the previous

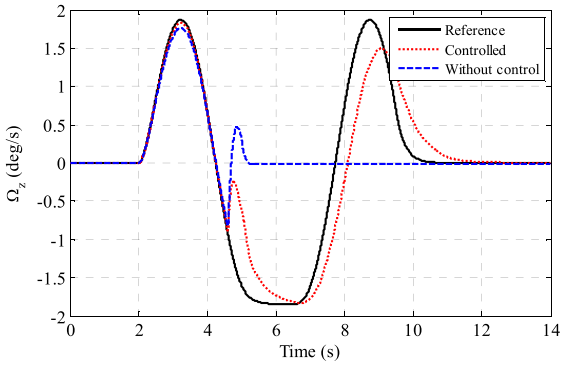

Fig. 14. Vehicle yaw rates in the double-lane change simulation.

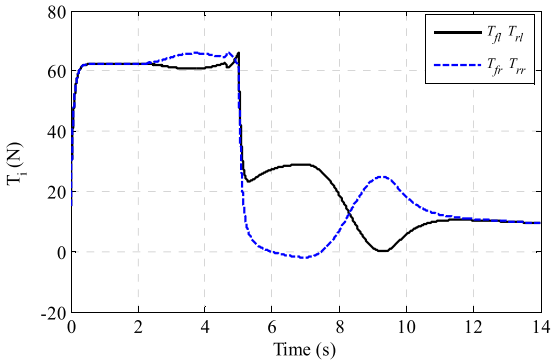

Fig. 15. Motor torque values in the double-lane change simulation (controlled vehicle).

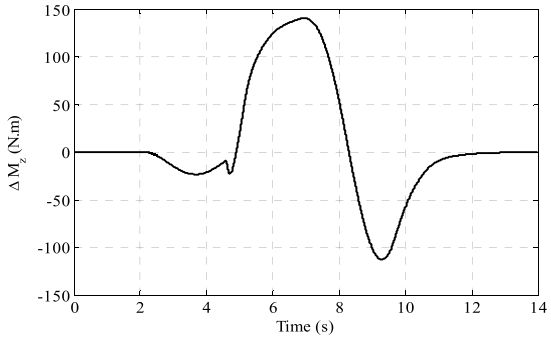

Fig. 16. External yaw moment generated with the tire force difference.

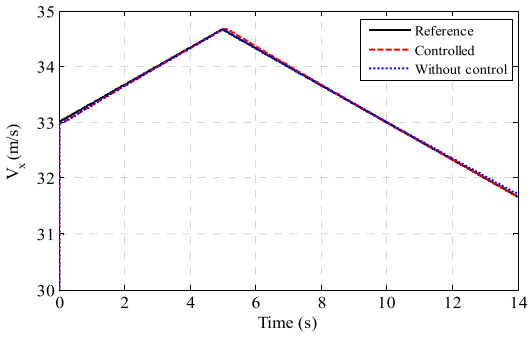

Fig. 17. Vehicle longitudinal speeds in the double-lane change simulation.

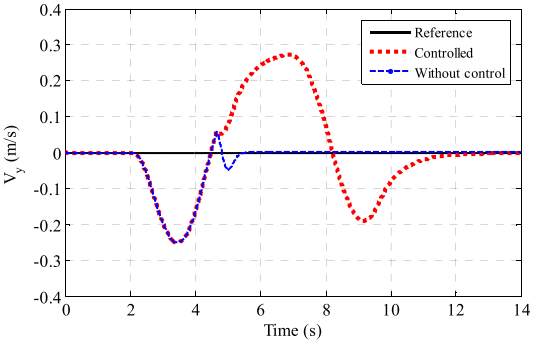

Fig. 18. Vehicle lateral speed in the double-lane change simulation.

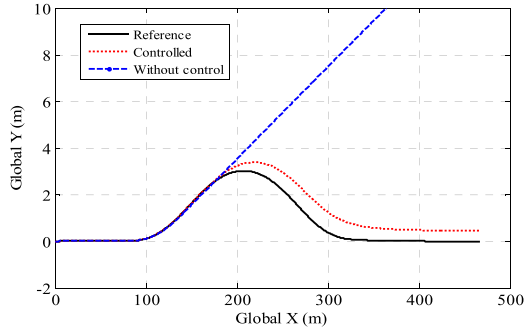

Fig. 19. Vehicle trajectories in the double-lane change simulation.

two cases. Because of the steering system failure, the control effectiveness of the steering system decreased to zero, which induced a zero ground-wheel steering angle. The vehicle's yaw rate in this case was controlled by the external yaw moment generated with the torque difference between the left and right in-wheel motors. Note that although a considerable tracking error existed, the controlled yaw rate could still move in the same trend of the reference. The motor torques and the external yaw moment generated with the in-wheel motor torque difference are shown in Figs. 15 and 16, respectively. One can see that as soon as the steering system fault was introduced, the external yaw moment increased to compensate the yaw rate tracking error.

The vehicle longitudinal speeds are shown in Fig. 17. As no in-wheel motor fault occurred in this case, the longitudinal speed of the uncontrolled vehicle could track the reference. The vehicle lateral speeds are plotted in Fig. 18, where one can see that the lateral speed of the uncontrolled vehicle converged to zero. Although the zero lateral speed shows zero sideslip angle of the vehicle, this does not necessarily mean that the lateral motion was well controlled. The zero lateral speed was caused by the zero ground-wheel steering angle induced by the failure of the steering system. The vehicle trajectories are shown in Fig. 19, from which we can see that uncontrolled vehicle ran in a straight line and deviated from the reference quickly once the ground-wheel steering angle became zero. We can also observe that a tracking error existed in vehicle lateral position. Although the control performance decreased compared with the previous two cases where the steering system control effectiveness partially lost, the control performance of the proposed FT controller is still acceptable.

It should be noted that when the vehicle deviates from the desired trajectory, the driver may give a corrective steering to control the vehicle yaw motion. As a matter of fact, the reaction lag of the driver could affect the vehicle lateral

motion considerably [8]. As the vehicle yaw rate will change fast when a fault occurs, the driver may become panic and give inappropriate steering action in practice, which may induce accidents. Also, for some fault scenarios, such as the steering system failure, the front wheel steering cannot be adjusted as the steering actuator will float with zero moment even if the suitable corrective steering action could be given by the driver. With the help of the proposed FT controller, external yaw moment can be generated with the torque difference between the left and right side motors to control the vehicle yaw motion, and acceptable control performance can be achieved. So FT controller in all fault and driving scenarios are necessary.

V. Conclusion

A passive FT robust LQR-based H_∞ controller using the LPV method is proposed to preserve closed-loop stability of an FWIA electric ground vehicles rather than in-wheel motors or/and steering system faults. Different types of actuator faults are considered simultaneously. With the LQR-based H_∞ control, the tradeoff between the tracking performance and the control input energy is achieved, and the effect from the external input to the controlled output is minimized. The uncertainties in the tire cornering stiffness are also considered in the FT controller design. Simulations using a high-fidelity, CarSim®, and full-vehicle model show that the vehicle can be well controlled if the steering system is not in a total failure.

Note that a total failure of the steering system decreases the FT control effectiveness. To obtain better control results when the steering system completely fails, an active FT controller may be required. Also note that a state feedback controller was used in this paper and the system states include the lateral speed. A dual-antenna GPS system or optical sensors, typically considered expensive for commercial vehicle applications, are required to measure the lateral speed, and this might be a limitation of the proposed controller. The output feedback FT controller, which can avoid the use of lateral speed information, will be investigated in future research. The preview actions [37] and the CAN-bus induced time delays [38], [39] will also be considered.

Appendix A

Rewriting $\boldsymbol{A}_{\xi c}(\boldsymbol{\rho})$ in (28) as

$$\boldsymbol{A}_{\xi c}(\boldsymbol{\rho}) = \boldsymbol{A}_{\xi 3}(\boldsymbol{\rho}) + \tilde{\boldsymbol{B}}_{\mathbf{ext}} \boldsymbol{N}_3 \tilde{\boldsymbol{\Lambda}} \boldsymbol{K}(\boldsymbol{\rho}) \tag{A1}$$

with

$$\boldsymbol{A}_{\xi 3}(\boldsymbol{\rho}) = \boldsymbol{A}_{\Xi}(\boldsymbol{\rho}) + \begin{bmatrix} \tilde{\boldsymbol{A}}(\boldsymbol{\rho}) + \tilde{\boldsymbol{B}} \\ \mathbf{0} \end{bmatrix} \boldsymbol{N_1} \left([\boldsymbol{I} \ \ \mathbf{0}] + \boldsymbol{\Lambda_m} \boldsymbol{K}(\boldsymbol{\rho}) \right) + \boldsymbol{B}_{\mathbf{ext}} \boldsymbol{N_2} \tilde{\boldsymbol{\Lambda}} \boldsymbol{K}(\boldsymbol{\rho})$$

we have

$$\boldsymbol{P}\boldsymbol{B}_{\xi c} = \boldsymbol{P}\left(\boldsymbol{B}_{\mathbf{ext}} + \tilde{\boldsymbol{B}}_{\mathbf{ext}} \boldsymbol{N}_1\right) = \boldsymbol{P}\boldsymbol{B}_{\mathbf{ext}} + \boldsymbol{P}\tilde{\boldsymbol{B}}_{\mathbf{ext}} \boldsymbol{N}_1 \tag{A2}$$

and

$$\begin{aligned} \boldsymbol{A}_{\xi c}^{\boldsymbol{T}}(\boldsymbol{\rho})\boldsymbol{P} + \boldsymbol{P}\boldsymbol{A}_{\xi c}(\boldsymbol{\rho}) &= \left(\boldsymbol{A}_{\xi 3}(\boldsymbol{\rho}) + \tilde{\boldsymbol{B}}_{\mathbf{ext}} \boldsymbol{N}_3 \tilde{\boldsymbol{\Lambda}} \boldsymbol{K}(\boldsymbol{\rho}) \right)^{\boldsymbol{T}} \boldsymbol{P} \\ &\quad + \boldsymbol{P}\left(\boldsymbol{A}_{\xi 3}(\boldsymbol{\rho}) + \tilde{\boldsymbol{B}}_{\mathbf{ext}} \boldsymbol{N}_3 \tilde{\boldsymbol{\Lambda}} \boldsymbol{K}(\boldsymbol{\rho}) \right) \\ &= \boldsymbol{A}_{\xi 3}^{\boldsymbol{T}}(\boldsymbol{\rho})\boldsymbol{P} + \boldsymbol{P}\boldsymbol{A}_{\xi 3}(\boldsymbol{\rho}) + \left(\tilde{\boldsymbol{\Lambda}} \boldsymbol{K}(\boldsymbol{\rho}) \right)^{\boldsymbol{T}} \boldsymbol{N}_{\boldsymbol{3}}^{\boldsymbol{T}} \left(\boldsymbol{P}\tilde{\boldsymbol{B}}_{\mathbf{ext}} \right)^{\boldsymbol{T}} \\ &\quad + \boldsymbol{P}\tilde{\boldsymbol{B}}_{\mathbf{ext}} \boldsymbol{N}_{\boldsymbol{3}} \tilde{\boldsymbol{\Lambda}} \boldsymbol{K}(\boldsymbol{\rho}). \end{aligned} \tag{A3}$$

Then the matrix inequality (35) can be rewritten as

$$\begin{aligned} &\begin{bmatrix} \boldsymbol{A}_{\xi c}^{\boldsymbol{T}}(\boldsymbol{\rho})\boldsymbol{P} + \boldsymbol{P}\boldsymbol{A}_{\xi c}(\boldsymbol{\rho}) & \boldsymbol{P}\boldsymbol{B}_{\xi c} & \boldsymbol{C}_{\xi c}^{\boldsymbol{T}} \\ * & -\boldsymbol{I} & \mathbf{0} \\ * & * & -\boldsymbol{\gamma}_{\boldsymbol{1}}^{\boldsymbol{2}}\boldsymbol{I} \end{bmatrix} \\ &= \begin{bmatrix} \boldsymbol{A}_{\xi 3}^{\boldsymbol{T}}(\boldsymbol{\rho})\boldsymbol{P} + \boldsymbol{P}\boldsymbol{A}_{\xi 3}(\boldsymbol{\rho}) & \boldsymbol{P}\boldsymbol{B}_{\mathbf{ext}} & \boldsymbol{C}_{\xi c}^{\boldsymbol{T}} \\ * & -\boldsymbol{I} & \mathbf{0} \\ * & * & -\boldsymbol{\gamma}_{\boldsymbol{1}}^{\boldsymbol{2}}\boldsymbol{I} \end{bmatrix} \\ &\quad + \begin{bmatrix} \boldsymbol{P}\tilde{\boldsymbol{B}}_{\mathbf{ext}} & \boldsymbol{P}\tilde{\boldsymbol{B}}_{\mathbf{ext}} \\ \mathbf{0} & \mathbf{0} \\ \mathbf{0} & \mathbf{0} \end{bmatrix} \begin{bmatrix} \boldsymbol{N}_3 & \mathbf{0} \\ \mathbf{0} & \boldsymbol{N}_1 \end{bmatrix} \begin{bmatrix} \tilde{\boldsymbol{\Lambda}} \boldsymbol{K}(\boldsymbol{\rho}) & \mathbf{0} & \mathbf{0} \\ \mathbf{0} & \boldsymbol{I} & \mathbf{0} \end{bmatrix} \\ &\quad + \begin{bmatrix} \left(\tilde{\boldsymbol{\Lambda}} \boldsymbol{K}(\boldsymbol{\rho}) \right)^{\mathbf{T}} & \mathbf{0} \\ \mathbf{0} & \boldsymbol{I} \\ \mathbf{0} & \mathbf{0} \end{bmatrix} \begin{bmatrix} \boldsymbol{N}_3 & \mathbf{0} \\ \mathbf{0} & \boldsymbol{N}_1 \end{bmatrix}^{T} \begin{bmatrix} \boldsymbol{P}\tilde{\boldsymbol{B}}_{\mathbf{ext}^T} & \mathbf{0} & \mathbf{0} \\ \boldsymbol{P}\tilde{\boldsymbol{B}}_{\mathbf{ext}^T} & \mathbf{0} & \mathbf{0} \end{bmatrix}. \end{aligned} \tag{A4}$$

It follows from Lemma 2 that (A5), as shown at the bottom of the page, holds. Repeat the above procedure and rewrite

$$\begin{aligned} \boldsymbol{A}_{\xi 3}^{\boldsymbol{T}}(\boldsymbol{\rho})\boldsymbol{P} + \boldsymbol{P}\boldsymbol{A}_{\xi 3}(\boldsymbol{\rho}) &= \left(\boldsymbol{A}_{\xi 2}(\boldsymbol{\rho}) + \tilde{\boldsymbol{B}}_{\mathbf{ext}} \boldsymbol{N}_2 \tilde{\boldsymbol{\Lambda}} \boldsymbol{K}(\boldsymbol{\rho}) \right)^{\boldsymbol{T}} \boldsymbol{P} \\ &\quad + \boldsymbol{P}\left(\boldsymbol{A}_{\xi 2}(\boldsymbol{\rho}) + \tilde{\boldsymbol{B}}_{\mathbf{ext}} \boldsymbol{N}_2 \tilde{\boldsymbol{\Lambda}} \boldsymbol{K}(\boldsymbol{\rho}) \right) \\ &= \boldsymbol{A}_{\xi 2}^{\boldsymbol{T}}(\boldsymbol{\rho})\boldsymbol{P} + \boldsymbol{P}\boldsymbol{A}_{\xi 2}(\boldsymbol{\rho}) + \left(\tilde{\boldsymbol{\Lambda}} \boldsymbol{K}(\boldsymbol{\rho}) \right)^{\boldsymbol{T}} \boldsymbol{N}_2^{\boldsymbol{T}} \left(\boldsymbol{P}\tilde{\boldsymbol{B}}_{\mathbf{ext}} \right)^{\boldsymbol{T}} \\ &\quad + \boldsymbol{P}\tilde{\boldsymbol{B}}_{\mathbf{ext}} \boldsymbol{N}_2 \tilde{\boldsymbol{\Lambda}} \boldsymbol{K}(\boldsymbol{\rho}) \end{aligned} \tag{A6}$$

with

$$\boldsymbol{A}_{\xi 2}^{\boldsymbol{T}}(\boldsymbol{\rho}) = \boldsymbol{A}_{\Xi}(\boldsymbol{\rho}) + \tilde{\boldsymbol{A}}_{\mathbf{ext}}(\boldsymbol{\rho}) \boldsymbol{N_1} [\boldsymbol{I} \ \ \mathbf{0}] + \tilde{\boldsymbol{B}}_{\mathbf{ext}} \boldsymbol{N_1} \boldsymbol{\Lambda_m} \boldsymbol{K}(\boldsymbol{\rho}). \tag{A7}$$

So, it follows from Lemma 2 that (A8), as shown at the top of the next page, holds. Based on (A7), repeating the above procedure twice, we get, the equation shown at top of the next page, where $\boldsymbol{\Xi} = \boldsymbol{A}_{\boldsymbol{\Xi}}^{\boldsymbol{T}}(\boldsymbol{\rho})\boldsymbol{P} + \boldsymbol{P}\boldsymbol{A}_{\boldsymbol{\Xi}}(\boldsymbol{\rho})$. Performing a

$$\begin{bmatrix} \boldsymbol{A}_{\xi 3}^{\boldsymbol{T}}(\boldsymbol{\rho})\boldsymbol{P} + \boldsymbol{P}\boldsymbol{A}_{\xi 3}(\boldsymbol{\rho}) & \boldsymbol{P}\boldsymbol{B}_{\mathbf{ext}} & \boldsymbol{C}_{\xi c}^{\boldsymbol{T}} & \varepsilon_1(\boldsymbol{\rho})\boldsymbol{P}\tilde{\boldsymbol{B}}_{\mathbf{ext}} & \varepsilon_2(\boldsymbol{\rho})\boldsymbol{P}\tilde{\boldsymbol{B}}_{\mathbf{ext}} & \left(\tilde{\boldsymbol{\Lambda}} \boldsymbol{K}(\boldsymbol{\rho})\right)^{T} & \mathbf{0} \\ * & -\boldsymbol{\gamma}_{\boldsymbol{1}}^{\boldsymbol{2}}\boldsymbol{I} & \mathbf{0} & \mathbf{0} & \mathbf{0} & \mathbf{0} & \varepsilon_2(\boldsymbol{\rho})\boldsymbol{I} \\ * & * & -\boldsymbol{I} & \mathbf{0} & \mathbf{0} & \mathbf{0} & \mathbf{0} \\ * & * & * & -\varepsilon_1(\boldsymbol{\rho})\boldsymbol{I} & \mathbf{0} & \mathbf{0} & \mathbf{0} \\ * & * & * & * & -\varepsilon_2(\boldsymbol{\rho})\boldsymbol{I} & \mathbf{0} & \mathbf{0} \\ * & * & * & * & * & -\varepsilon_1(\boldsymbol{\rho})\boldsymbol{I} & \mathbf{0} \\ * & * & * & * & * & * & -\varepsilon_2(\boldsymbol{\rho})\boldsymbol{I} \end{bmatrix} < \mathbf{0} \tag{A5}$$

$$\begin{bmatrix} \boldsymbol{A}_{\xi 2}^{\mathbf{T}}(\boldsymbol{\rho})\boldsymbol{P}+\boldsymbol{P}\boldsymbol{A}_{\xi 2}(\boldsymbol{\rho}) & \boldsymbol{P}\boldsymbol{B}_{\mathbf{ext}} & \boldsymbol{C}_{\xi \mathbf{c}}^{T} & \varepsilon_1(\boldsymbol{\rho})\boldsymbol{P}\tilde{\boldsymbol{B}}_{\mathbf{ext}} & \varepsilon_2(\boldsymbol{\rho})\boldsymbol{P}\tilde{\boldsymbol{B}}_{\mathbf{ext}} & (\tilde{\boldsymbol{\Lambda}}\boldsymbol{K}(\boldsymbol{\rho}))^{T} & \mathbf{0} & \varepsilon_3(\boldsymbol{\rho})\boldsymbol{P}\tilde{\boldsymbol{B}}_{\mathbf{ext}} & (\tilde{\boldsymbol{\Lambda}}\boldsymbol{K}(\boldsymbol{\rho}))^{T} \\ * & -\gamma_1^2\boldsymbol{I} & \mathbf{0} & \mathbf{0} & \mathbf{0} & \mathbf{0} & \varepsilon_2(\boldsymbol{\rho})\boldsymbol{I} & \mathbf{0} & \mathbf{0} \\ * & * & \boldsymbol{I} & \mathbf{0} & \mathbf{0} & \mathbf{0} & \mathbf{0} & \mathbf{0} & \mathbf{0} \\ * & * & * & -\varepsilon_1(\boldsymbol{\rho})\boldsymbol{I} & \mathbf{0} & \mathbf{0} & \mathbf{0} & \mathbf{0} & \mathbf{0} \\ * & * & * & * & -\varepsilon_2(\boldsymbol{\rho})\boldsymbol{I} & \mathbf{0} & \mathbf{0} & \mathbf{0} & \mathbf{0} \\ * & * & * & * & * & -\varepsilon_1(\boldsymbol{\rho})\boldsymbol{I} & \mathbf{0} & \mathbf{0} & \mathbf{0} \\ * & * & * & * & * & * & -\varepsilon_2(\boldsymbol{\rho})\boldsymbol{I} & \mathbf{0} & \mathbf{0} \\ * & * & * & * & * & * & * & -\varepsilon_3(\boldsymbol{\rho})\boldsymbol{I} & \mathbf{0} \\ * & * & * & * & * & * & * & * & -\varepsilon_3(\boldsymbol{\rho})\boldsymbol{I} \end{bmatrix} < \mathbf{0} \quad \text{(A8)}$$

$$\begin{bmatrix} \boldsymbol{\Xi} & \boldsymbol{P}\boldsymbol{B}_{\mathbf{ext}} & \mathbf{C}_{\xi \mathbf{c}}^{T} & \varepsilon_1(\boldsymbol{\rho})\boldsymbol{P}\tilde{\boldsymbol{B}}_{\mathbf{ext}} & \varepsilon_2(\boldsymbol{\rho})\boldsymbol{P}\tilde{\boldsymbol{B}}_{\mathbf{ext}} & (\tilde{\boldsymbol{\Lambda}}\boldsymbol{K}(\boldsymbol{\rho}))^{T} & \mathbf{0} & \varepsilon_3(\boldsymbol{\rho})\boldsymbol{P}\tilde{\boldsymbol{B}}_{\mathbf{ext}} & (\tilde{\boldsymbol{\Lambda}}\boldsymbol{K}(\boldsymbol{\rho}))^{T} & \varepsilon_5(\boldsymbol{\rho})\boldsymbol{P}\tilde{\boldsymbol{B}}_{\mathbf{ext}} & (\boldsymbol{\Lambda}_m\boldsymbol{K}(\boldsymbol{\rho}))^{T} & \varepsilon_6(\boldsymbol{\rho})\boldsymbol{P}\tilde{\boldsymbol{A}}_{\mathbf{ext}} & \boldsymbol{I}_{\mathbf{ext}} \\ * & -\gamma_1^2\boldsymbol{I} & \mathbf{0} & \mathbf{0} & \mathbf{0} & \mathbf{0} & \varepsilon_2(\boldsymbol{\rho})\boldsymbol{I} & \mathbf{0} & \mathbf{0} & \mathbf{0} & \mathbf{0} & \mathbf{0} & \mathbf{0} \\ * & * & \boldsymbol{I} & \mathbf{0} & \mathbf{0} & \mathbf{0} & \mathbf{0} & \mathbf{0} & \mathbf{0} & \mathbf{0} & \mathbf{0} & \mathbf{0} & \mathbf{0} \\ * & * & * & -\varepsilon_1(\boldsymbol{\rho})\boldsymbol{I} & \mathbf{0} & \mathbf{0} & \mathbf{0} & \mathbf{0} & \mathbf{0} & \mathbf{0} & \mathbf{0} & \mathbf{0} & \mathbf{0} \\ * & * & * & * & -\varepsilon_2(\boldsymbol{\rho})\boldsymbol{I} & \mathbf{0} & \mathbf{0} & \mathbf{0} & \mathbf{0} & \mathbf{0} & \mathbf{0} & \mathbf{0} & \mathbf{0} \\ * & * & * & * & * & -\varepsilon_1(\boldsymbol{\rho})\boldsymbol{I} & \mathbf{0} & \mathbf{0} & \mathbf{0} & \mathbf{0} & \mathbf{0} & \mathbf{0} & \mathbf{0} \\ * & * & * & * & * & * & -\varepsilon_2(\boldsymbol{\rho})\boldsymbol{I} & \mathbf{0} & \mathbf{0} & \mathbf{0} & \mathbf{0} & \mathbf{0} & \mathbf{0} \\ * & * & * & * & * & * & * & -\varepsilon_3(\boldsymbol{\rho})\boldsymbol{I} & \mathbf{0} & \mathbf{0} & \mathbf{0} & \mathbf{0} & \mathbf{0} \\ * & * & * & * & * & * & * & * & -\varepsilon_3(\boldsymbol{\rho})\boldsymbol{I} & \mathbf{0} & \mathbf{0} & \mathbf{0} & \mathbf{0} \\ * & * & * & * & * & * & * & * & * & -\varepsilon_4(\boldsymbol{\rho})\boldsymbol{I} & \mathbf{0} & \mathbf{0} & \mathbf{0} \\ * & * & * & * & * & * & * & * & * & * & -\varepsilon_4(\boldsymbol{\rho})\boldsymbol{I} & \mathbf{0} & \mathbf{0} \\ * & * & * & * & * & * & * & * & * & * & * & -\varepsilon_5(\boldsymbol{\rho})\boldsymbol{I} & \mathbf{0} \\ * & * & * & * & * & * & * & * & * & * & * & * & -\varepsilon_5(\boldsymbol{\rho})\boldsymbol{I} \end{bmatrix} < \mathbf{0}$$

$$\begin{bmatrix} -r\boldsymbol{Q} & q\boldsymbol{Q}+\boldsymbol{A}_{\Xi}(\boldsymbol{\rho})\boldsymbol{Q} & \varepsilon_{10}(\boldsymbol{\rho})\tilde{\boldsymbol{B}}_{\mathbf{ext}} & \mathbf{0} & \varepsilon_{11}(\boldsymbol{\rho})\boldsymbol{B}_{\mathbf{ext}} & \mathbf{0} & \varepsilon_{12}(\boldsymbol{\rho})\tilde{\boldsymbol{B}}_{\mathbf{ext}} & \mathbf{0} & \varepsilon_{13}(\boldsymbol{\rho})\tilde{\boldsymbol{A}}_{\mathbf{ext}}(\boldsymbol{\rho}) & \mathbf{0} \\ * & -r\boldsymbol{Q} & \mathbf{0} & \boldsymbol{H}^{T}\tilde{\boldsymbol{\Lambda}} & \mathbf{0} & \boldsymbol{H}^{T}\tilde{\boldsymbol{\Lambda}} & \mathbf{0} & \boldsymbol{H}^{T}\tilde{\boldsymbol{\Lambda}}_m & \mathbf{0} & \boldsymbol{Q}\boldsymbol{I}_{\mathbf{ext}} \\ * & * & -\varepsilon_{10}(\boldsymbol{\rho})\boldsymbol{I} & \mathbf{0} & \mathbf{0} & \mathbf{0} & \mathbf{0} & \mathbf{0} & \mathbf{0} & \mathbf{0} \\ * & * & * & -\varepsilon_{10}(\boldsymbol{\rho})\boldsymbol{I} & \mathbf{0} & \mathbf{0} & \mathbf{0} & \mathbf{0} & \mathbf{0} & \mathbf{0} \\ * & * & * & * & -\varepsilon_{11}(\boldsymbol{\rho})\boldsymbol{I} & \mathbf{0} & \mathbf{0} & \mathbf{0} & \mathbf{0} & \mathbf{0} \\ * & * & * & * & * & -\varepsilon_{11}(\boldsymbol{\rho})\boldsymbol{I} & \mathbf{0} & \mathbf{0} & \mathbf{0} & \mathbf{0} \\ * & * & * & * & * & * & -\varepsilon_{12}(\boldsymbol{\rho})\boldsymbol{I} & \mathbf{0} & \mathbf{0} & \mathbf{0} \\ * & * & * & * & * & * & * & -\varepsilon_{12}(\boldsymbol{\rho})\boldsymbol{I} & \mathbf{0} & \mathbf{0} \\ * & * & * & * & * & * & * & * & -\varepsilon_{13}(\boldsymbol{\rho})\boldsymbol{I} & \mathbf{0} \\ * & * & * & * & * & * & * & * & * & -\varepsilon_{13}(\boldsymbol{\rho})\boldsymbol{I} \end{bmatrix} < \mathbf{0} \quad \text{(A12)}$$

congruence transformation with $\Gamma = \text{diag}[\boldsymbol{Q} \quad \underbrace{\boldsymbol{I} \ldots \boldsymbol{I}}_{12}]$ to the above inequality, we get (43) holds. The inequality in (44) can be proved in a similar way.

Now we are in the position to prove that the inequality in (45) holds. It follows from Lemma 3 that

$$\begin{bmatrix} -r\boldsymbol{Q} & q\boldsymbol{Q}+\boldsymbol{A}_{\xi c}(\boldsymbol{\rho})\boldsymbol{Q} \\ * & -r\boldsymbol{Q} \end{bmatrix} < 0. \quad \text{(A9)}$$

As $\boldsymbol{A}_{\xi c}(\boldsymbol{\rho}) = \boldsymbol{A}_{\xi 3}(\boldsymbol{\rho}) + \tilde{\boldsymbol{B}}_{\mathbf{ext}}\boldsymbol{N}_3\tilde{\boldsymbol{\Lambda}}\boldsymbol{K}(\boldsymbol{\rho})$, following from Lemma 2, we have

$$\begin{bmatrix} -r\boldsymbol{Q} & q\boldsymbol{Q}+\boldsymbol{A}_{\xi 3}(\boldsymbol{\rho})\boldsymbol{Q} & \varepsilon_{10}\tilde{\boldsymbol{B}}_{\mathbf{ext}} & \mathbf{0} \\ * & -r\boldsymbol{Q} & \mathbf{0} & \boldsymbol{H}^{T}\tilde{\boldsymbol{\Lambda}} \\ * & * & -\varepsilon_{10}\boldsymbol{I} & \mathbf{0} \\ * & * & * & -\varepsilon_{10}\boldsymbol{I} \end{bmatrix} < 0. \quad \text{(A10)}$$

As $\boldsymbol{A}_{\xi 3}(\boldsymbol{\rho}) = \boldsymbol{A}_{\xi 2}(\boldsymbol{\rho}) + \tilde{\boldsymbol{B}}_{\mathbf{ext}}\boldsymbol{N}_2\tilde{\boldsymbol{\Lambda}}\boldsymbol{K}(\boldsymbol{\rho})$, repeating the above process, we have

$$\begin{bmatrix} -r\boldsymbol{Q} & q\boldsymbol{Q}+\boldsymbol{A}_{\xi 2}(\boldsymbol{\rho})\boldsymbol{Q} & \varepsilon_{10}\tilde{\boldsymbol{B}}_{\mathbf{ext}} & \mathbf{0} & \varepsilon_{11}\boldsymbol{B}_{\mathbf{ext}} & \mathbf{0} \\ * & -r\boldsymbol{Q} & \mathbf{0} & \boldsymbol{H}^{T}\tilde{\boldsymbol{\Lambda}} & \mathbf{0} & \boldsymbol{H}^{T}\tilde{\boldsymbol{\Lambda}} \\ * & * & -\varepsilon_{10}\boldsymbol{I} & \mathbf{0} & \mathbf{0} & \mathbf{0} \\ * & * & * & -\varepsilon_{10}\boldsymbol{I} & \mathbf{0} & \mathbf{0} \\ * & * & * & * & -\varepsilon_{11}\boldsymbol{I} & \mathbf{0} \\ * & * & * & * & * & -\varepsilon_{11}\boldsymbol{I} \end{bmatrix} < 0. \quad \text{(A11)}$$

Similarly, as $\boldsymbol{A}_{\xi 2}(\boldsymbol{\rho}) = \boldsymbol{A}_{\Xi}(\boldsymbol{\rho}) + \tilde{\boldsymbol{A}}_{\text{ext}}(\boldsymbol{\rho})\boldsymbol{N}_1\boldsymbol{I}_{\text{ext}}^{T} + \tilde{\boldsymbol{B}}_{\mathbf{ext}}\boldsymbol{N}_1\boldsymbol{\Lambda}_m\boldsymbol{K}(\boldsymbol{\rho})$, we get (A12), as shown at the top of the page, from Lemma 2. The proof is finished.

Appendix B

Based on (46), (43) can be rewritten as

$$\sum_{i=1}^{7}\theta_i^2\boldsymbol{\Pi}_{1ii} + \sum_{i=1}^{7}\theta_i\sum_{j=i+1}^{8}\theta_j\left(\boldsymbol{\Pi}_{1ij}+\boldsymbol{\Pi}_{1ji}\right). \quad \text{(B1)}$$

Similarly, we can write (44) and (45) as

$$\sum_{i=1}^{7}\theta_i^2\boldsymbol{\Pi}_{2ii} + \sum_{i=1}^{7}\theta_i\sum_{j=i+1}^{8}\theta_j\left(\boldsymbol{\Pi}_{2ij}+\boldsymbol{\Pi}_{2ji}\right)$$
$$\sum_{i=1}^{7}\theta_i^2\boldsymbol{\Pi}_{3ii} + \sum_{i=1}^{7}\theta_i\sum_{j=i+1}^{8}\theta_j\left(\boldsymbol{\Pi}_{3ij}+\boldsymbol{\Pi}_{3ji}\right). \quad \text{(B2)}$$

One can claim that if (50) is achievable, the inequalities in (43)–(45) hold, and the gain-scheduling controller can ensure stability of the controlled system. This completes the proof.

REFERENCES

[1] J. Wang and R. G. Longoria, "Coordinated and reconfigurable vehicle dynamics control," *IEEE Trans. Control Syst. Technol.*, vol. 17, no. 3, pp. 723–732, May 2009.

[2] M. Shino and M. Nagai, "Independent wheel torque control of small-scale electric vehicle for handling and stability improvement," *JSAE Rev.*, vol. 24, no. 4, pp. 449–456, Oct. 2003.

[3] R. Wang and J. Wang, "Stability control of electric vehicles with four independently actuated wheels," in *Proc. 50th IEEE Conf. Decision Control Eur. Control Conf.*, Dec. 2011, pp. 2511–2516.

[4] N. M. Enache, M. Netto, S. Mammar, and B. Lusetti, "Driver steering assistance for lane departure avoidance," *Control Eng. Pract.*, vol. 17, no. 6, pp. 642–651, Jun. 2009.

[5] N. M. Enache, S. Mammar, M. Netto, and B. Lusetti, "Driver steering assistance for lane-departure avoidance based on hybrid automata and composite Lyapunov function," *IEEE Trans. Intell. Transp. Syst.*, vol. 11, no. 1, pp. 28–39, Mar. 2010.

[6] B. Zheng, C. Altemare, and S. Anwar, "Fault tolerant steer-by-wire road wheel control system," in *Proc. Amer. Control Conf.*, Jun. 2005, pp. 1619–1624.

[7] R. Wang and J. Wang, "Fault-tolerant control with active fault diagnosis for four-wheel independently-driven electric ground vehicles," *IEEE Trans. Veh. Technol.*, vol. 60, no. 9, pp. 4276–4287, Nov. 2011.

[8] R. Wang and J. Wang, "Fault-tolerant control for electric ground vehicles with independently-actuated in-wheel motors," *ASME Trans. J. Dyn. Syst., Meas., Control*, vol. 134, no. 2, pp. 021014-1–021014-10, Jan. 2012.

[9] J. Hua, D. Yin, and Y. Hori, "Fault-tolerant traction control of electric vehicles," *Control Eng. Pract.*, vol. 19, no. 2, pp. 204–213, Feb. 2011.

[10] C. Poussot-Vassal, O. Sename, L. Dugard, and S. M. Savaresi, "Vehicle dynamic stability improvements through gain-scheduled steering and braking control," *Veh. Syst. Dyn.*, vol. 49, no. 10, pp. 1597–1621, Mar. 2011.

[11] R. Jayabalan and B. Fahimi, "Monitoring and fault diagnosis of multi-converter systems in hybrid electric vehicles," *IEEE Trans. Veh. Technol.*, vol. 55, no. 5, pp. 1475–1484, Sep. 2006.

[12] R. Isermann, R. Schwartz, and S. Stolzl, "Fault-tolerant drive-by-wire systems," *IEEE Control Syst. Mag.*, vol. 27, no. 5, pp. 64–81, Oct. 2002.

[13] Y. Chen and J. Wang, "Design and experimental evaluations on energy efficient control allocation methods for over-actuated electric vehicles: Longitudinal motion case," *IEEE/ASME Trans. Mech.*, 2013, DOI: 10.1109/TMECH.2013.2249591.

[14] H. Yang, V. Cocquempot, and B. Jiang, "Optimal fault-tolerant path-tracking control for 4WS4WD electric vehicles," *IEEE Trans. Intell. Transp. Syst.*, vol. 11, no. 1, pp. 237–243, Mar. 2010.

[15] Y. Zhang and J. Jiang, "Bibliographical review on reconfigurable fault-tolerant control systems," *Annu. Rev. Control*, vol. 32, no. 2, pp. 229–252, Dec. 2008.

[16] B. Zheng and S. Anwar, "Fault-tolerant control of the road wheel subsystem in a steer-by-wire system," *Int. J. Veh. Technol.*, vol. 2008, pp. 1–8, Jan. 2008.

[17] J. Pimentel, "An architecture for a safety-critical steer-by-wire system," Kettering Univ., Flint, MI, USA, SAE Tech. Rep. 2004-01-0714, Jan. 2004.

[18] S. Anwar and L. Chen, "An analytical redundancy-based fault detection and isolation algorithm for a road-wheel control subsystem in a steer-by-wire system," *IEEE Trans. Veh. Technol.*, vol. 56, no. 5, pp. 2857–2859, Sep. 2007.

[19] N. Meskin and K. Khorasani, "Fault detection and isolation of actuator faults in overactuated systems," in *Proc. Amer. Control Conf.*, Jul. 2007, pp. 2527–2532.

[20] J. Y. Wong, *Theory of Ground Vehicles*, 3rd ed. New York, NY, USA: Wiley, 2001.

[21] R. Wang and J. Wang, "Tire–road friction coefficient and tire cornering stiffness estimation based on longitudinal tire force difference generation," *Control Eng. Pract.*, vol. 21, no. 1, pp. 65–75, Jan. 2013.

[22] J. O. Hahn, R. Rajamani, and L. Alexander, "GPS-based real-time identification of tire-road friction coefficient," *IEEE Trans. Control Syst. Technol.*, vol. 10, no. 3, pp. 331–343, May 2002.

[23] R. N. Jazar, *Vehicle Dynamics: Theory and Applications*. New York, NY, USA: Springer-Verlag, 2008.

[24] H. Zhang, Y. Shi, and A. S. Mehr, "Robust non-fragile dynamic vibration absorbers with uncertain factors," *J. Sound Vibrat.*, vol. 330, no. 4, pp. 559–566, Feb. 2011.

[25] H. Zhang, Y. Shi, and A. S. Mehr, "Robust H_∞ PID control for multivariable networked control systems with disturbance/noise attenuation," *Int. J. Robust Nonlinear Control*, vol. 22, no. 2, pp. 183–204, Jan. 2012.

[26] H. Zhang, Y. Shi, and A. S. Mehr, "Robust static output feedback control and remote PID design for networked motor systems," *IEEE Trans. Ind. Electron.*, vol. 58, no. 12, pp. 5396–5405, Dec. 2011.

[27] W. Xie, "An equivalent LMI representation of bounded real lemma for continuous-time systems," *J. Inequalities Appl.*, vol. 2008, pp. 1–8, Jan. 2008.

[28] H. Zhang, Y. Shi, and A. S. Mehr, "Robust energy-to-peak filtering for networked systems with time-varying delays and randomly missing data," *IET Control Theory Appl.*, vol. 4, no. 12, pp. 2921–2936, Dec. 2010.

[29] M. Chilali and P. Gahinet, "H_∞ design with pole placement constraints: An LMI approach," *IEEE Trans. Autom. Control*, vol. 41, no. 3, pp. 358–367, Mar. 1996.

[30] R. Wang, Y. Chen, D. Feng, X. Huang, and J. Wang, "Development and performance characterization of an electric ground vehicle with independently actuated in-wheel motors," *J. Power Sour.*, vol. 196, no. 8, pp. 3962–3971, Apr. 2011.

[31] Y. Chen and J. Wang, "Design and evaluation on electric differentials for over-actuated electric ground vehicles with four independent in-wheel motors," *IEEE Trans. Veh. Technol.*, vol. 61, no. 4, pp. 1534–1542, May 2012.

[32] J. Ahmadi, A. K. Sedigh, and M. Kabganian, "Adaptive vehicle lateral-plane motion control using optimal tire friction forces with saturation limits consideration," *IEEE Trans. Veh. Technol.*, vol. 58, no. 8, pp. 4098–4107, Oct. 2009.

[33] H. P. Du, N. Zhang, and G. M. Dong, "Stabilizing vehicle lateral dynamics with considerations of parameter uncertainties and control saturation through robust yaw control," *IEEE Trans. Veh. Technol.*, vol. 59, no. 5, pp. 2593–2597, Jun. 2010.

[34] S. Horiuchi, K. Okada, and S. Nohtomi, "Improvement of vehicle handling by nonlinear integrated control of four wheel steering and four wheel torque," *JSAE Rev.*, vol. 20, no. 4, pp. 459–464, Oct. 1999.

[35] R. Wang and J. Wang, "Passive actuator fault-tolerant control for a class of over-actuated nonlinear systems and applications to electric Vehicles," *IEEE Trans. Veh. Technol.*, vol. 62, no. 3, pp. 972–985, Mar. 2013.

[36] H. Zhang, Y. Shi, and A. S. Mehr, "Parameter-dependent mixed H_2/H_∞ filtering for linear parameter-varying systems," *IET Signal Process.*, vol. 6, no. 7, pp. 697–703, Sep. 2012.

[37] H. Zhang, Y. Shi, and B. X. Mu, "Optimal H_∞-based linear-quadratic regulator tracking control for discrete-time Takagi–Sugeno fuzzy systems with preview actions," *J. Dyn. Syst., Meas., Control*, vol. 135, no. 4, pp. 044501-1–044501-5, May 2013.

[38] H. Zhang, Y. Shi, and M. X. Liu, "H_∞ step tracking control for networked discrete-time nonlinear systems with integral and predictive actions," *IEEE Trans. Ind. Inf.*, vol. 9, no. 1, pp. 337–345, Feb. 2013.

[39] H. Zhang, Y. Shi, and J. Wang, "Observer-based tracking controller design for networked predictive control systems with uncertain Markov delays," *Int. J. Control*, 2013, DOI: 10.1080/00207179.2013.797107.

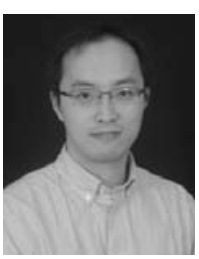

Rongrong Wang received the B.E. degree in control science and engineering from Tianjin University, Tianjin, China, in 2006, and the B.S degree in economics from Nankai University, Tianjin, in 2006, the M.S. degree in control science and engineering from Tsinghua University, Beijing, China, in 2009, and the Ph.D. degree in mechanical engineering from The Ohio State University, Columbus, OH, USA, in 2013.

He is currently an Associate Professor with the School of Mechanical Engineering, Southeast University, Nanjing, China. His current research interests include nonlinear systems control, fault-tolerant control, and vehicle dynamics and control.

Hui Zhang received the B.Sc. degree in mechanical design manufacturing and automation from the Harbin Institute of Technology at Weihai, Weihai, China, in 2006, the M.Sc. degree in automotive engineering from Jilin University, Changchun, China, in 2008, and the Ph.D. degree in mechanical engineering from the University of Victoria, Victoria, BC, Canada, in 2012.

He is currently a Post-Doctoral Researcher with the Department of Mechanical and Aerospace Engineering, The Ohio State University, Columbus, OH, USA. He has authored or co-authored of over 30 peer-reviewed papers on journals and conference proceedings. His current research interests include diesel engine after treatment systems, vehicle dynamics and control, robust control and filtering, networked control systems, and signal processing.

Dr. Zhang has served on the IFAC Junior Technical Committee on Automotive Control, the ASME Automotive and Transportation Systems Technical Committee, the SAE Commercial Vehicle Committee, and the International Program Committee for the IASTED International Conference on Control and Applications.

Junmin Wang (M'06) received the B.E. degree in automotive engineering and the M.S. degree in power machinery and engineering from Tsinghua University, Beijing, China, in 1997 and 2000, respectively, the second and third M.S. degrees in electrical engineering and mechanical engineering from the University of Minnesota, Twin Cities, MN, USA, in 2003, and the Ph.D. degree in mechanical engineering from the University of Texas at Austin, Austin, TX, USA, in 2007.

He has five-years of full-time industrial research experience with Southwest Research Institute, San Antonio, TX, USA, from 2003 to 2008. In 2008, he joined Ohio State University, Columbus, OH, USA, and founded the Vehicle Systems and Control Laboratory. He is the author or co-author of more than 150 peer-reviewed journal and conference papers and holds 11 U.S. patents. His current research interests include control, modeling, estimation, and diagnosis of dynamical systems, specifically for engine, powertrain, aftertreatment, hybrid, flexible fuel, alternative/renewable energy, (electric) ground vehicle, transportation, sustainable mobility, energy storage, and mechatronic systems.

Dr. Wang serves as an Associate Editor for the IEEE TRANSACTIONS ON VEHICULAR TECHNOLOGY and *SAE International Journal of Engines*. He served as the Chair of the SAE International Control and Calibration Committee from 2010 to 2012, and is the Vice Chair of the ASME Automotive and Transportation Systems Technical Committee from 2012 to 2014, and a Vice Chair (Automotive) of the IFAC Technical Committee on Mechatronic Systems. He is a recipient of the SAE Ralph R. Teetor Educational Award in 2012, the National Science Foundation CAREER Award in 2012, the Ohio State University Lumley Research Award in 2012, the 2009 SAE International Vincent Bendix Automotive Electronics Engineering Award in 2011, the Office of Naval Research Young Investigator Program Award in 2009, and the ORAU Ralph E. Powe Junior Faculty Enhancement Award in 2009.